IOPscience iopscience.iop.org

Home Search Collections Journals About Contact us My IOPscience

Phenomenology of the normal state in-plane transport properties of high-T_c cuprates

This article has been downloaded from IOPscience. Please scroll down to see the full text article.

2008 J. Phys.: Condens. Matter 20 123201

(http://iopscience.iop.org/0953-8984/20/12/123201)

View the table of contents for this issue, or go to the journal homepage for more

Download details:
IP Address: 129.252.86.83
The article was downloaded on 29/05/2010 at 11:09

Please note that terms and conditions apply.

IOP PUBLISHING JOURNAL OF PHYSICS: CONDENSED MATTER

J. Phys.: Condens. Matter **20** (2008) 123201 (17pp) doi:10.1088/0953-8984/20/12/123201

TOPICAL REVIEW

Phenomenology of the normal state in-plane transport properties of high-T_c cuprates

N E Hussey

H H Wills Physics Laboratory, Tyndall Avenue, Bristol BS8 1TL, UK

E-mail: n.e.hussey@bristol.ac.uk

Received 6 November 2007, in final form 20 December 2007
Published 25 February 2008
Online at stacks.iop.org/JPhysCM/20/123201

Abstract

In this article, I review progress towards an understanding of the normal state (in-plane) transport properties of high-T_c cuprates in the light of recent developments in both spectroscopic and transport measurement techniques. Against a backdrop of mounting evidence for anisotropic single-particle lifetimes in cuprate superconductors, new results have emerged that advocate similar momentum dependence in the transport decay rate $\Gamma(\mathbf{k})$. In addition, enhancement of the energy scale (up to the bare bandwidth) over which spectroscopic information on the quasiparticle response can be obtained has led to the discovery of new, unforeseen features that, surprisingly, may have a significant bearing on the transport properties at the dc limit. With these two key developments in mind, I consider here whether all the ingredients necessary for a complete phenomenological description of the anomalous normal state transport properties of high-T_c cuprates are now in place.

(Some figures in this article are in colour only in the electronic version)

Contents

1. Introduction 1
2. Electronic structure 2
3. In-plane resistivity 3
4. In-plane Hall coefficient 4
5. In-plane magnetoresistance 6
6. The theoretical landscape 7
7. Anisotropic quasiparticle scattering 8
8. Scattering rate saturation 11
9. Discussion and conclusions 13
Acknowledgments 15
References 15

1. Introduction

As it enters its third decade, the field of high temperature superconductivity is finally leaving behind the heady days of adolescence. As a sign of its growing maturity, it is slowly beginning to reveal more of its dark secrets under the watchful gaze of dedicated experimentalists whose techniques have been honed almost uniquely in response to this, one of the most profound problems in contemporary physics [1]. Angle-resolved photoemission spectroscopy (ARPES) and scanning tunnelling microscopy (STM) are arguably the two most high-profile examples of techniques whose measurements on cuprates have undergone remarkable progress, but there are others, such as inelastic neutron scattering (INS), that have enjoyed a similar transformation in recent years.

The improved momentum k and energy ϵ resolution of both ARPES and STM (the latter achieving its k dependence via Fourier-transform scanning tunnelling spectroscopy) have opened up new vistas on the physics of the in-plane quasiparticles, that have revealed, amongst other discoveries, a remarkable 'dichotomy' between the nodal and anti-nodal eigenstates [2, 3]. This development has been supplemented by recent enhancement in the energy ranges in both ARPES and INS over which the excitation spectra can be probed, up to

 © 2008 IOP Publishing Ltd Printed in the UK

energies of the order of the bare bandwidth W [4–8] and the exchange interaction J [9, 10] respectively.

Within the transport community, the ability to resolve small spectral weight differences between the normal and superconducting states (the so-called Ferrell–Glover–Tinkham sum rule) is testimony to the improvement in quality of optical conductivity data (and its analysis) in recent years [11–13]. This has also led to a similar extension of the energy scale for probing the quasiparticle response [14] and the development of methods to extract bosonic spectral densities across the full energy range [15]. Raman spectroscopy is now providing k resolution on scattering processes and excitations through careful polarization selection [16], whilst the application of angle-dependent magnetoresistance (ADMR) techniques to overdoped cuprates has unravelled for the first time different components of the in-plane transport scattering rate [17–19].

With this striking progress in the field over the last few years, it appears timely to take stock of the growing body of experimental evidence and to assess to what extent our understanding of charge dynamics in the cuprates has improved. In this topical review, I choose to focus on the normal state in-plane dc transport properties, resistivity, Hall effect and magnetoresistance, but consider the output from a range of different experimental probes and how such information might impact on our understanding of the cuprate transport problem.

The subject is important for a number of reasons. Just as in conventional superconductors, where the electron–phonon scattering processes that dominate the electrical resistivity provided an important clue to the pairing interaction, so an understanding of the normal state transport properties of high-T_c cuprates (HTCs) is widely regarded as a key step towards the elucidation of the pairing mechanism for high-temperature superconductivity. Whilst this remains the ultimate goal, the anomalous transport behaviour of the cuprates themselves has become arguably the most studied phenomenon in the field of correlated electrons, a phenomenon that has inspired and engaged, at some point or other, all but a fraction of the global condensed matter theoretical community [20]. And as experimentalists slowly unravel more of the details, so the consensus of the theoretical community seems to be migrating away from non-Fermi-liquid based models towards more Fermi-liquid-like 'variations on a theme'. Given this apparent paradigm shift, it therefore seems prudent to examine to what extent conventional electronic band structure calculations and the quasiparticle picture in general can account for the myriad of transport phenomena observed.

The article is arranged as follows. For the benefit of those new to the field, I begin by introducing the electronic band structure of cuprates, before summarizing the key experimental observations, focusing on data that are generic to most cuprates and for the most part obtained on bulk single crystals. This is followed by a general discussion of the current theoretical landscape and a review of recent transport and spectroscopic measurements that shed new light on an old problem. I chose not to include detailed or comprehensive modelling in this paper; the task is simply to catalogue those ingredients I believe to be necessary for a coherent phenomenological description of charge transport in HTC. As this is a topical review, I focus on the most recent articles in the field and, in acknowledging the vast amount of literature that has helped to shape the problem over the past two decades, I apologize for their exclusion from this article.

2. Electronic structure

The structural element common to all HTCs is the square planar CuO_2 plaquette shown schematically in figure 1(a). Holes (or electrons) are doped onto the copper oxide planes from the charge reservoir layers located between them. A combination of covalency, crystal field splitting and Jahn–Teller distortion then combine to create an electronic structure whose highest partially filled band has predominantly $Cu3d_{x^2-y^2}$ and $O2p_{x,y}$ character. The resulting two-dimensional (2D) energy dispersion can be expressed in tight-binding representation as

$$\epsilon(\mathbf{k}) = \epsilon_0 - 2t(\cos k_x + \cos k_y) + 4t'(\cos k_x \cdot \cos k_y) - 2t''(\cos 2k_x + \cos 2k_y). \quad (1)$$

At half-filling, with only nearest-neighbour (t) hopping, a diamond-like Fermi surface (FS) is expected. Inclusion of next-nearest-neighbour (t') hopping leads to a more rounded topology. Pavarini *et al* identified an intriguing correlation between T_c and the ratio t'/t for a large number of cuprate families [21]. Low-T_c cuprates like $La_{2-x}Sr_xCuO_4$ (LSCO) and $Bi_2Sr_{2-x}La_xCuO_6$ (Bi-2201) have a relatively low t'/t, whilst those with higher T_c values, such as $Bi_2Sr_2CaCu_2O_{8+\delta}$ (Bi2212), $YBa_2Cu_3O_{7-\delta}$ (YBCO) and $Tl_2Ba_2CuO_{6+\delta}$ (Tl2201), have much more rounded FS geometries characteristic of the higher t'/t values. These predictions have largely been verified by extensive ARPES measurements [22]. The differences in topology are highlighted in figures 1(b) and (c) where representative 2D FS projections of LSCO and Tl2201 respectively are shown for two different doping levels $p = 0.15$ (near optimal doping) and 0.30 (beyond the superconducting dome). As one can see, the lower t'/t values in LSCO have the effect of driving the Fermi level ϵ_F below the van Hove singularity, inducing a crossover from a hole-like to an electron-like FS, at a doping level of approximately $p = 0.18$ [23]. In the other cuprates, this does not occur, except perhaps for the anti-bonding band in Bi2212 [24]. As I shall demonstrate here, these differences in FS topology are reflected in the dc transport properties.

Local density approximation (LDA) band structure calculations were largely ignored at the beginning of the HTC era due to the failure of LDA to account for the antiferromagnetic insulating phase of the parent compound. However, recent years have brought substantial improvement in theoretical techniques that include strong correlations in first-principles approaches. Moreover, a combination of new-generation ARPES [25] and ADMR [26] has revealed that many details of the original LDA calculations are in fact reproduced experimentally, particularly in the more highly doped cuprates ($p > 0.15$). The correct fermiology of weakly doped cuprates, on the other hand, is still to be resolved; whilst no-one disputes the existence of a (pseudo)gap in the normal

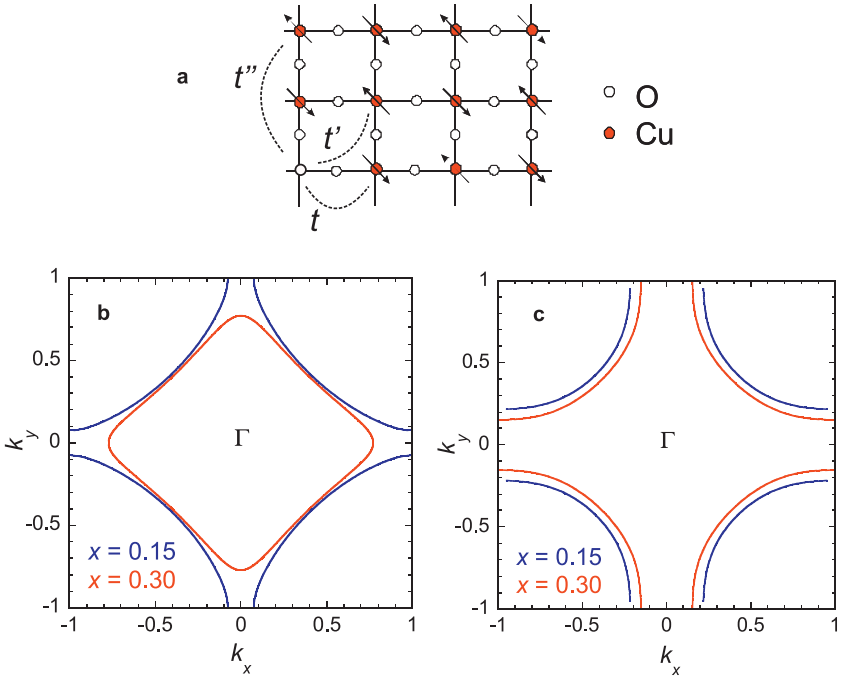

Figure 1. (a) Schematic figure of the CuO_2 plane showing the spin alignments of the Cu spins at half-filling within the basal plane and the three principal hopping parameters t, t' and t''. (b) Schematic 2D projection of the Fermi surface in $La_{2-x}Sr_xCuO_4$ for $p = 0.15$ ($t'/t = 0.15$) and 0.30 ($t'/t = 0.12$). (c) Similar projections for $Tl_2Ba_2CuO_{6+\delta}$ for $p = 0.15$ ($t'/t = 0.22$) and 0.30 ($t'/t = 0.22$). In all cases, $t''/t' = -0.5$.

state excitation spectrum, its manifestation on the (remnant) FS and its evolution with temperature and doping remain highly controversial [27, 28]. In light of this, I will focus here more on the highly doped regions of the phase diagram, though I shall return to discuss the situation in underdoped cuprates at the end.

3. In-plane resistivity

The in-plane resistivity $\rho_{ab}(T)$ of hole-doped HTCs shows a very systematic evolution with doping, that is summarized in figure 2, where a schematic phase diagram of p-type cuprates is reproduced together with the doping and temperature evolution of $\rho_{ab}(T)$. (Electron-doped cuprates will be dealt with at the end of this section.) The solid lines are the phase boundaries between the normal state and the superconducting or antiferromagnetic ground state, whilst the dashed lines indicate (ill defined) crossovers in $\rho_{ab}(T)$ behaviour, each of which may or may not be associated with a fundamental change in the nature of the electronic states. Optimal doping is indicated by the vertical dotted line corresponding to the pinnacle of the superconducting dome, and the areas to the left (right) of this line are the underdoped (overdoped) regions of the phase diagram respectively.

In the underdoped (UD) cuprates, $\rho_{ab}(T)$ varies approximately linearly with temperature at high T, but as the temperature is lowered $\rho_{ab}(T)$ deviates downward from linearity due to the partial removal of a dominant scattering channel, as evidenced by the drop in $1/\tau(\omega)$ seen in infrared spectroscopy [29]. This change of slope in $\rho_{ab}(T)$ was initially

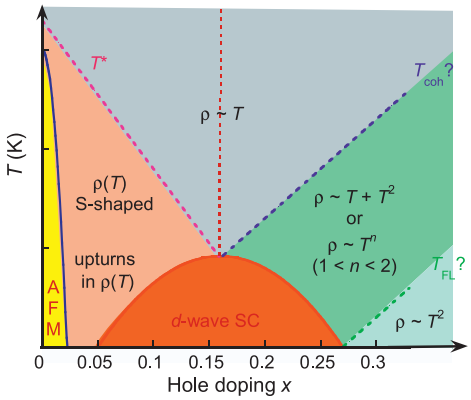

Figure 2. Phase diagram of (hole-doped) cuprates mapped out in terms of the temperature and doping evolution of the in-plane resistivity $\rho_{ab}(T)$. The solid lines are the phase boundaries between the normal state and the superconducting or antiferromagnetic ground state. The dashed lines indicate (ill defined) crossovers in $\rho_{ab}(T)$ behaviour. The meanings of the labels T^*, T_{coh} and T_{FL} are explained in the text.

interpreted as a 'kink' in $\rho_{ab}(T)$ at $T = T^*$ (marked on the figure) [30, 31]. Plots of the derivative $d\rho_{ab}/dT$ showed however that $\rho_{ab}(T)$ in fact first deviates from linearity at a much higher T [32]. Moreover, in the vicinity of T^*, there is no additional feature in $d\rho_{ab}/dT$; the change of slope is a very gradual, continuous process with no clear evidence of a phase transition below T^*. In the more anisotropic cuprates such as LSCO [33] and Bi-2212 [34], it has proven difficult to distinguish between deviations from linearity due

Table 1. ρ_{ab} (300 K), normalized ρ_{ab} (300 K) and ρ_c/ρ_{ab} (T_c) values for some optimally doped cuprates.

Compound	$\rho_\parallel$ ($T = 300$ K) ($\mu\Omega$ cm)	$\rho_\parallel$/layer (300 K) ($\mu\Omega$ cm)	$\rho_\perp/\rho_\parallel$ (T_c)
$YBa_2Cu_3O_{6.95}$	290 [39]	580	3×10^1 [40]
$La_{1.83}Sr_{0.17}CuO_4$	420 [39]	420	3×10^2 [41]
$Bi_2Sr_{1.61}La_{0.39}CuO_6$	500 [39]	500	1×10^6 [42]
$Bi_2Sr_2CaCu_2O_{8+\delta}$	280 [43]	560	1×10^5 [43]
$Tl_2Ba_2CuO_{6+\delta}$	450 [44]	450	2×10^3 [45]

to genuine pseudogap effects and those due to paraconductivity fluctuations near T_c. The dashed line depicting T^* in figure 1 reflects this ill defined nature.

At sufficiently low temperatures, $\rho_{ab}(T)$ of UD cuprates develops an upturn, suggestive of some form of (as yet unidentified) electronic localization. This upturn is characterized by a marked $\log(1/T)$ dependence [35]. The critical doping level p_{crit} at which these upturns occur differs amongst the various cuprate families, being close to optimal doping in LSCO [36], at one-eighth doping in La-doped Bi2201 [37] and close to the insulator/superconducting boundary in YBCO [38]. This trend towards lower p_{crit} with increasing purity suggests that the onset of localization is in fact disorder driven.

Optimally doped (OP) cuprates are characterized by a T-linear resistivity that survives for all $T > T_c$. Despite the large variations in (optimal) T_c and in the crystallography of individual cuprate families, T-linear resistivity is a universal feature at optimal doping, confirming that it is intrinsic to the CuO_2 planes. Moreover, as illustrated in table 1, the value of ρ_{ab} at $T = 300$ K normalized to a single CuO_2 plane is largely independent of the chemical composition of the charge transfer layers. By contrast, the electrical anisotropy ρ_c/ρ_{ab} varies by approximately five orders of magnitude between the different families of cuprates (see table 1). The ρ_{ab} values themselves are large when compared with conventional superconductors. Given that the dc resistivity (conductivity) depends on both the normal state plasma frequency Ω_{pn}^2 ($=ne^2/\epsilon_0 m^*$ in a Drude picture, where n is the carrier density and m^* the effective mass) and the transport scattering rate $1/\tau_{tr} = \Gamma$, it has proved difficult to conclude whether these high values are due to a small coherent spectral weight, i.e. a small number of carriers with long lifetimes, or a large number of heavily damped quasiparticles. Recent analysis of optical conductivity data however does seems to suggest the latter [46].

In low-T_c OP cuprates, where the superconductivity can be destroyed by large magnetic fields, the T-linear $\rho_{ab}(T)$ has been found to cross over to a higher-power T dependence, eventually levelling off at some finite residual value [36, 37]. In higher-T_c OP cuprates, where this is not possible, a higher-power T dependence as $T \to 0$ can also be inferred from the fact that the slope of the T-linear resistivity often extrapolates to a *negative* intercept [44, 47]. Thus the T-linear resistivity observed in OP cuprates does *not* extend down to the lowest temperatures, at least not with the same slope. Moreover, Ando *et al* recently showed that the region of strict T-linearity (in the normal state) is rather narrow, concentrated at or around optimal doping [39]. This confinement of the T-linear resistivity to a narrow composition range near optimal doping is more suggestive of electron correlation effects than strong phonon interactions and is often regarded as a signature of quantum criticality, as demonstrated in the heavy-fermion compounds [48].

On the overdoped (OD) side, $\rho_{ab}(T)$ contains a significant supralinear contribution that can be interpreted either as a sum of two components, one T-linear, the other quadratic, or a single power law T^n where n varies smoothly from one at optimal doping to two at the SC/non-SC boundary on the OD side [45, 49, 50]. At sufficiently high T however, $\rho_{ab}(T)$ becomes T-linear once more. This crossover temperature [50] is marked in figure 2 as a coherence temperature T_{coh}, in line with the suggestion from the ARPES community that the onset of T-linear resistivity coincides with the loss of the qp (coherence) peak in the energy dispersion curves [51].

The crossover to purely quadratic $\rho_{ab}(T)$, characteristic of a correlated Fermi liquid (FL), is only observed beyond the superconducting dome. In heavily OD, non-superconducting $La_{1.7}Sr_{0.3}CuO_4$ for example, the low-T resistivity in zero field is found to be purely quadratic up to $T = 50$ K [52]. The dashed line marked T_{FL} represents this crossover to strictly T^2 resistivity, and, whilst its nomenclature hints at conventional FL behaviour, quantum oscillations, the classic signature of a FL, have never been observed in this region of the phase diagram. Significantly, Mackenzie *et al* measured $\rho_{ab}(T)$ of heavily OD Tl2201 down to 0.1 K, suppressing T_c (=15 K) with a large magnetic field, and still found evidence for a finite T-linear term coexisting with this T^2 term and surviving into the $T = 0$ limit [49]. Such behaviour is manifestly non-Fermi-liquid-like.

In marked contrast to what is observed in hole-doped cuprates, doping appears to have little or no effect on the T dependence of $\rho_{ab}(T)$ in n-type cuprates such as $Pr_{2-x}Ce_xCuO_{4+\delta}$ (PCCO), at least in the intermediate-temperature regime (100 K $\leqslant T \leqslant$ 300 K) [53]. At low temperatures however, $\rho_{ab}(T)$ becomes highly sensitive to changes in cerium and oxygen content with both metallic and insulating behaviour being reported [54–56]. As shown in figure 3(a), a T-linear resistivity is also observed in slightly overdoped PCCO between 30 K and 40 mK [54], reminiscent of what is seen in OD Tl2201 [49]. Finally, a recent doping-dependent study revealed that the limiting low-T form of $\rho_{ab}(T)$ could be expressed as $\rho_{ab}(T) = \rho_0 + AT^\beta$, with β tending to unity at a critical doping level $x_c = 0.165$, again suggestive of a quantum critical point near optimal doping [55].

4. In-plane Hall coefficient

The in-plane Hall coefficient R_H of hole-doped cuprates varies markedly with both p and T. This behaviour is encapsulated by data on LSCO by Hwang *et al* [57], which spans the entire (hole-doped) phase diagram from the Mott insulator to the non-superconducting metal. These data are reproduced in figures 3(b) and (c) for UD and OD LSCO respectively [57]. At optimal doping ($x \sim 0.15$), R_H is found to vary approximately

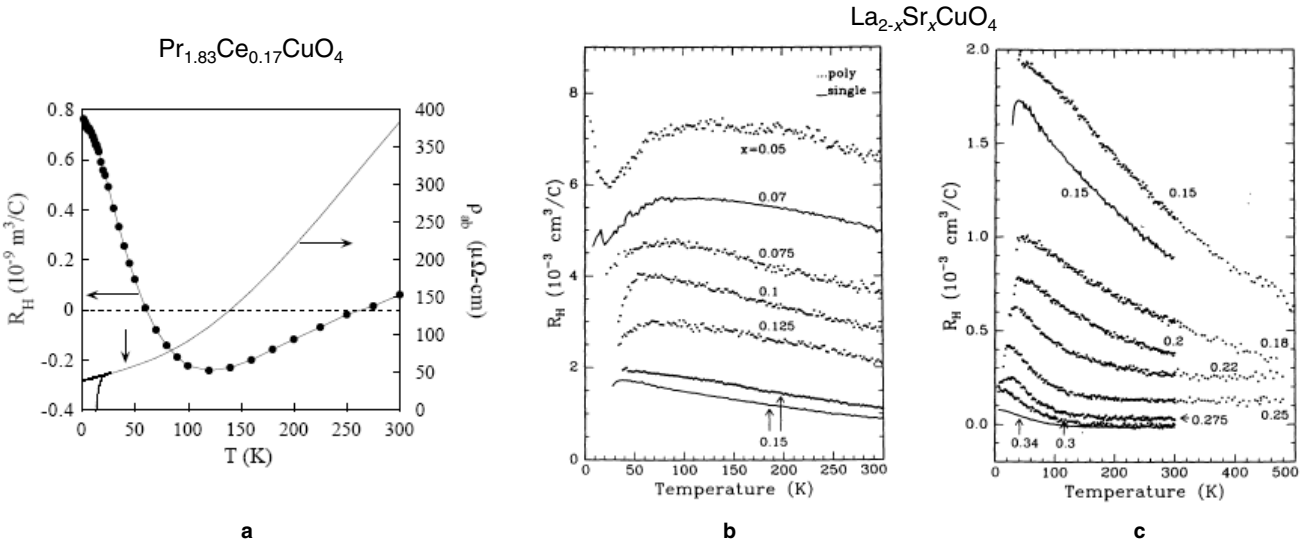

Figure 3. (a) In-plane resistivity $\rho_{ab}(T)$ and Hall coefficient $R_H(T)$ data for a slightly overdoped $Pr_{1.83}Ce_{0.17}CuO_4$ thin film. Reprinted with kind permission from [54], figure 4. Copyright 1998 by the American Physical Society. (b) $R_H(T)$ for underdoped $La_{2-x}Sr_xCuO_4$. (c) $R_H(T)$ for overdoped $La_{2-x}Sr_xCuO_4$. Reprinted with kind permission from [57], figure 4. Copyright 1994 by the American Physical Society.

as $1/T$ over a wide temperature range [58], in apparent violation of conventional Fermi-liquid theory.

According to band structure calculations, a 'large' FS containing $(1 + x)$ holes/Cu ion is predicted, centred around the corners of the Brillouin zone as shown in figure 1. In the UD region, however, the carrier density n_H at low T, estimated from the Drude relation $R_H = 1/n_H e$, approaches the 'chemical' hole concentration x deduced from the formal valence of Cu^{2+x} [59–61]. The observed scaling of R_H with x thus appears to suggest a violation of the Luttinger sum rule and either the presence of 'small' Fermi pockets containing x holes or a series of Fermi arcs with an active (ungapped) arc length proportional to x. At higher doping levels, R_H falls more rapidly (by two orders of magnitude for $0.05 < x < 0.25$ [59–61]), possibly reflecting the crossover from a small to a large FS. Finally, for $x > 0.25$, $R_H(T)$ becomes negative at elevated T [57].

Recent results from ARPES [23, 62, 63] support the doping evolution of the FS in LSCO inferred from Hall measurements. At very low x, a weak but well defined quasiparticle peak appears around the nodal point that forms into an 'arc' whose intensity increases smoothly with increasing x [63] consistent with the variation of the carrier number n. Beyond optimal doping, spectral intensity is strong everywhere on the FS [23] and ϵ_F moves below the saddle near $(\pi, 0)$, leading to a topological shift from a hole-like to an electron-like FS [62], as shown in figure 2.

Despite this apparent consistency between the spectroscopic and transport probes, several outstanding issues remain, in particular the magnitude and sign of R_H at low T. Whilst ARPES suggests that the FS in LSCO is electron-like for $x \geqslant 0.18$, R_H $(T \to 0)$ remains positive at all doping levels up to $x = 0.34$ [57, 64]. Given that they are, for the most part, single-band metals, this sign problem is troublesome, since at low T, where scattering is dominated by impurities, the mean free path ℓ is expected to become independent of momentum $\mathbf{k}$. In this so-called isotropic-ℓ regime, $R_H(0)$ for a two-dimensional (2D) single-band metal should reflect the sign of the dominant carrier, even if there are electron- and hole-like patches of FS [65], with a magnitude equal to the Drude result $1/ne$.

At high T, R_H values in HTCs agree roughly with LDA calculations. Thus, there appears to be a crossover from the high-T band-like regime to a low-T anomalous regime. The crossover temperature T_{RH} systematically increases with decreasing hole concentration [57, 59]. A close correlation has been pointed out between T_{RH} and the onset temperature of AFM correlations T_χ, defined as a temperature where the uniform susceptibility starts showing a rapid decrease, thereby implying a possible link between the AFM spin correlations and the unusual behaviour of $R_H(T)$ [57, 59]. Recent high-temperature measurements of R_H in underdoped LSCO by Ono and Ando [66] however suggest that this strong T dependence at lower doping levels is in fact evidence for activated behaviour across the charge transfer gap that persists over a wide doping and temperature range [67].

In electron-doped cuprates, $R_H(T)$ shows all the hallmarks of a system containing electron- *and* hole-like carriers [68]. At low doping R_H is negative and strongly T dependent, but around optimal doping $R_H(T)$ changes sign, sometimes more than once, as the temperature is lowered. An example is shown in figure 3(a) for OP PCCO [54]. In this doping region, the Hall resistivity ρ_{xy} also displays strong non-linearity with magnetic field B, and at certain temperatures can even change sign with increasing B [69]. Finally, in the OD regime, R_H becomes positive and only weakly T dependent. This evolution with doping mirrors that of the fermiology of n-type cuprates as deduced from ARPES. At low doping, the Fermi surface is an electron pocket centred around $(\pi, 0)$, with a volume proportional to x, the other regions in $\mathbf{k}$-space being gapped presumably by spin-density-wave formation [70, 71]. Upon further doping, spectral weight eventually appears along

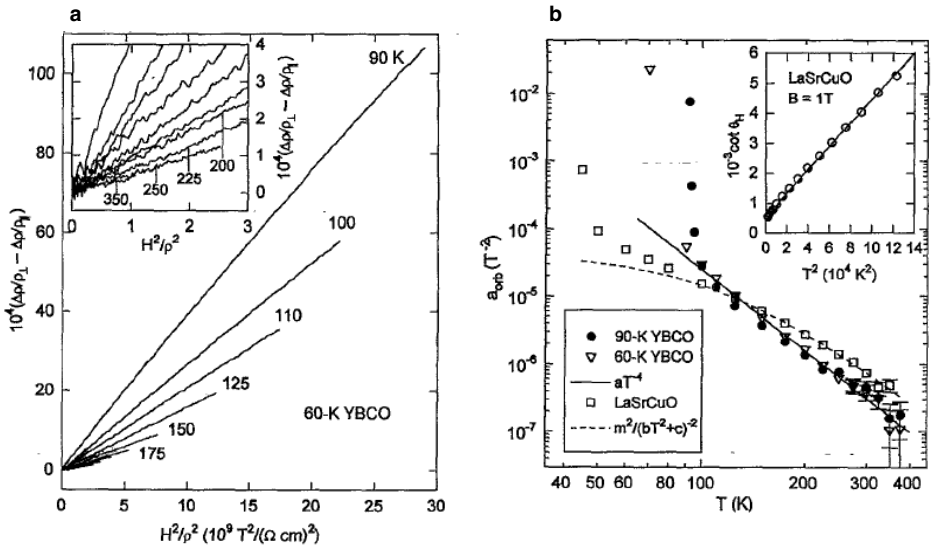

Figure 4. (a) Kohler plot for underdoped $YBa_2Cu_3O_{6.6}$ at intermediate (main) and high (inset) temperatures. Reprinted with kind permission from [78], figure 4. Copyright 1995 by the American Physical Society. (b) Temperature dependence of the orbital part of the magnetoresistance in $YBa_2Cu_3O_{6.6}$, optimally doped $YBa_2Cu_3O_7$ and $La_{1.85}Sr_{0.15}CuO_4$. The inset shows the inverse Hall angle $\cot\theta_H$ versus T^2 in OP LSCO. Reprinted with kind permission from [78], figure 3. Copyright 1995 by the American Physical Society.

the diagonal, giving rise to the two-carrier behaviour. Finally, as one moves beyond optimal doping, the two sets of pockets merge into a large hole-like Fermi surface with a volume $\sim 1 - x$ [72].

The relevance of the Hall coefficient as a gauge of carrier density and its evolution with temperature, particularly in the hole-doped cuprates, was challenged by the discovery that the inverse Hall angle $\cot\theta_H$ ($=\rho_{ab}/R_H B$) had a unique and distinct T dependence of its own [73]. In marked contrast to the T-linear resistivity (at optimal doping), $\cot\theta_H(T)$ shows a quadratic T dependence over a remarkably broad temperature range. In OP LSCO, for example, $\cot\theta_H(T) \sim A + BT^2$ between 50 and 400 K [57, 66] whilst $\rho_{ab} \propto T$ up to 1000 K [74]. This implicit 'separation of lifetimes' is a classic hallmark of the cuprates, and has led theorists to develop a number of radical ideas beyond conventional Fermi-liquid theory, some of which will be outlined below.

Finally, whilst the T^2 dependence of $\cot\theta_H$ holds for a wide range of doping in most cuprates, it is not the case for the Bi-based cuprates Bi2212 and Bi2201. In these systems, the power exponent of $\cot\theta_H(T)$ is closer to 1.75 than 2 [75, 76]. Detailed transport studies of both crystalline and thin-film samples of Bi2212 and Bi2201 have shown in fact that $\cot\theta_H(T) \sim A + BT^\alpha$ with α steadily decreasing from $\sim$2 to $\sim$1.6–1.7 as one moves from the UD to the OD regime [75, 76]. This variable power law behaviour in $\cot\theta_H(T)$ reveals a high level of complexity in the phenomenology of normal state transport in HTCs that has yet to be properly addressed.

5. In-plane magnetoresistance

According to Boltzmann transport theory, the orbital transverse magnetoresistance (MR) of a metal $\Delta\rho/\rho \propto (\omega_c\tau_{tr})^2$ where ω_c is the cyclotron frequency and τ_{tr} the transport lifetime. If the only effect of a change of temperature or of a change of purity of the metal is to alter $\tau_{tr}(\mathbf{k})$ to $\lambda\tau_{tr}(\mathbf{k})$, where λ is not a function of $\mathbf{k}$, then $\Delta\rho/\rho$ is unchanged if B is changed to B/λ. Thus the product $\Delta\rho \cdot \rho (= \Delta\rho/\rho \cdot \rho^2)$ is independent of τ_{tr} and a plot of $\Delta\rho/\rho$ versus $(B/\rho)^2$ is expected to fall on a straight line with a slope that is independent of T (provided the carrier concentration remains constant [77]). This relation, known as Kohler's rule, is obeyed in a large number of standard metals, including those with two types of carriers, provided that changes in temperature or purity simply alter $\tau_{tr}(\mathbf{k})$ by the same factor. In HTCs, however, the conventional Kohler's rule is strongly violated; instead of the data collapsing onto a single curve, there is a marked increase in the slope with decreasing temperature, as illustrated in the left panel of figure 4 for UD $YBa_2Cu_3O_{6.6}$ [78]. Remarkably, this progression continues up to 350 K (see inset).

Progress towards understanding this anomalous behaviour came in the form of a modified Kohler's rule suggested by Ong and co-workers [78]. They found that the in-plane orbital MR $\Delta\rho_{ab}/\rho_{ab}(T)$ follows the T dependence of $\tan^2\theta_H$ in both YBCO and LSCO much more closely than ρ_{ab}^2. The right panel of figure 4 shows the temperature dependence of the orbital MR in UD YBCO, OP YBCO and OP LSCO. The solid and dashed lines represent the T dependence of $\tan^2\theta_H$ for both OP samples. Similar scaling was also reported in OD Tl2201 [79]. Intriguingly, only in OD non-superconducting LSCO is conventional Kohler's scaling seemingly recovered [80].

Finally, in analysing the normal state orbital MR, one must not overlook contributions to the orbital MR from paraconductivity terms which can influence the in-plane magnetotransport over a wide temperature range in HTCs due to their small superconducting coherence length and strong two-dimensionality. In highly anisotropic Bi2212, for example, apparent Kohler's law violation up to 300 K can be

attributed almost entirely to superconducting fluctuations [81], whilst in UD YBCO fluctuation contributions are believed to persist up to temperatures of the order of T^* [82]. For a comprehensive review of fluctuation effects in HTCs, please refer to [83].

6. The theoretical landscape

The origin of the strong T dependence of R_H and its large magnitude at low doping have been the subjects of intense debate within the community. In a simple Drude picture, the sharp rise in $R_H(T)$ suggests a loss of carriers with decreasing temperature, due perhaps to the opening of the pseudogap [77, 84] or proximity to a vHs [85]. From this perspective, the non-monotonic $R_H(T)$ observed in most cuprates at low doping (see, e.g., figure 3(b)) ought only be interpreted as a repopulation of states. This conclusion however is not supported by magnetic susceptibility or specific heat data, that show a suppression of low energy states with decreasing temperature [86]. In a conventional metal, a strong T dependence of R_H can also arise due to multiple band effects. While this is evident in the electron-doped cuprates [54] and other multiple band quasi-2D metals such as Sr_2RuO_4 [87], it is unlikely to be applicable to the majority of hole-doped cuprates where the transport is dominated by a single band.

Attempts to explain the anomalous behaviour of $\rho_{ab}(T)$ and $R_H(T)$ in cuprates within a FL scenario have thus centred around the assumption of a (single) transport scattering rate whose magnitude varies around the in-plane FS. In-plane anisotropy in $1/\tau_{tr}$ has been attributed to anisotropic e–e (Umklapp) scattering [88] as well as to coupling to a singular bosonic mode, be it spin fluctuations [89, 90], charge fluctuations [91], d-wave superconducting fluctuations [92] or, more recently, Pomeranchuk fluctuations [93]. Generating a clear 'separation of lifetimes' within such single lifetime scenarios however has proved very difficult, requiring as it does a very subtle balancing act between different regions in k space with distinct T dependences. In the 'cold spots' model of Ioffe and Millis for example, the phenomenological scattering rate contains two terms, an isotropic FL scattering rate $1/\tau_{FL} \sim T^2$ and a T-independent scattering rate $1/\tau_0$, that is large everywhere except the nodal directions [92]. Whilst this model correctly explains the T-linear resistivity and quadratic Hall angle, the anisotropy required to separate the transport and Hall lifetimes gives rise to an orbital MR that is one order of magnitude too large and has a much stronger T dependence than is observed. These discrepancies can be resolved by the introduction of a 'shunt' scattering rate maximum Γ_{max}, which acts to reduce the overall effective anisotropy [88]. A modified Kohler's rule of the correct magnitude is then reproduced, but again its success relies heavily on a subtle balancing of anisotropies in the elastic and inelastic channels.

Given this reliance on detail, other more exotic models, based on non-FL physics, have gained prominence within the community: most notably, the two-lifetime picture of Anderson [94] and the marginal Fermi-liquid (MFL) phenomenology of Varma and co-workers [95]. In the two-lifetime approach, scattering processes involving momentum transfer perpendicular and parallel to the FS are governed by independent transport and Hall scattering rates $1/\tau_{tr}$ ($\propto T$) and $1/\tau_H$ ($\propto T^2$). In conventional FLs, of course, τ_{tr} is equal to τ_H. Allowing τ_H to be independent of τ_{tr}, the inverse Hall angle can now be written as $\cot\theta_H = \sigma_{xx}/\sigma_{xy} \propto 1/\tau_H$. Thus the different behaviour of $\rho_{ab}(T)$ and $\cot\theta_H(T)$ reflects the different T dependences of $1/\tau_{tr}$ and $1/\tau_H$. The enhancement of R_H then comes from the fact that τ_H becomes larger than τ_{tr} at low T. This model received strong support from Hall measurements on Zn-doped YBCO that showed $\cot\theta_H = A + BT^2$ to be robust to Zn doping with B remaining constant and A increasing in proportion to the Zn concentration [73], suggesting that the T^2 (inverse) Hall angle is a well defined fundamental quantity representing $1/\tau_H$. Later measurements on Co-doped YBCO [89] together with MR measurements on YBCO and LSCO [78] appeared to affirm the robustness of $1/\tau_H$. In particular, the T dependence of the MR could be quantitatively explained by modifying Kohler's rule such that $\rho_{ab}/\rho_{ab} \propto (\omega_c \cdot \tau_H)^2 \propto 1/(A + BT^2)^2$ and consequently $(\rho_{ab}/\rho_{ab})/\tan^2\theta_H$ became a constant.

Whilst the two-lifetime model of Anderson and co-workers has been successful in reproducing the experimental situation in OP cuprates, it does not appear to be consistent with ARPES results and has yet to explain the evolution of the transport phenomena across the full HTC phase diagram. The MFL hypothesis argues that the optimum T_c lies in proximity to a quantum critical point and, as a result, qp weight vanishes logarithmically at the FS, with the corresponding imaginary part of the self-energy governed simply by the temperature scale [95]. In contrast to the two-lifetime picture, MFL theory assumes a single T-linear scattering rate but introduces an unconventional expansion in the magnetotransport response. The Hall angle, for example, is given by the square of the transport lifetime [96], an idea that has received empirical support from infrared optical Hall angle studies [97]. In order to account for the observed magnetotransport behaviour in cuprates, Varma and Abrahams introduced anisotropy into their MFL phenomenology via the *elastic* (impurity) scattering rate by assuming small angle scattering off impurities located away from the CuO_2 plane [96]. Whilst this hypothesis seems consistent with certain ARPES measurements [98] *and* transport measurements [99] (see below), the legitimacy of the expansion in small scattering angle used in [96] has been subsequently challenged [100, 101]. In particular, it has been argued that the conditions that lead to a separation in lifetimes do *not* reproduce the violation of Kohler's rule [101]. Moreover, although the predictions of MFL theory appear compatible with the empirical situation in OP cuprates, their applicability to the rest of the cuprate phase diagram is less evident. In particular, the gradual convergence of the T dependences of $\rho_{ab}(T)$ and $\cot\theta_H(T)$ in OD cuprates sits uncomfortably with the idea of τ_H scaling with the square of the transport lifetime.

Thus, at the time of writing, none of the leading proposals appear to stand up to close scrutiny with the full complement of experimental data. It appears there is still some way to go before a coherent theoretical description of transport in HTCs can emerge and, if the truth be told, little progress has

been made over the last few years. On the experimental side, however, there have been a number of recent investigations that could ultimately lead to major advances in our comprehension of the origin of the anomalous transport properties and of the character of the qp scattering, both as a function of momentum and energy. In the following sections, I summarize these results, starting with evidence for anisotropic scattering, and discuss the impact of such findings on our interpretation of the dc normal state transport.

7. Anisotropic quasiparticle scattering

Evidence for T-dependent basal-plane anisotropy in the transport scattering rate in HTCs first came from studies of the angle-dependent interlayer magnetoresistance $\Delta\rho_c/\rho_c$ in OD Tl2201 [79]. On rotating the magnetic field B within the basal plane, $\Delta\rho_c/\rho_c$ was found to exhibit fourfold anisotropy with an amplitude that scaled as B^4 in accordance with Boltzmann transport analysis for an anisotropic quasi-2D FS. The ratio of the amplitude of these fourfold oscillations to the size of the higher order B^4 term in the isotropic MR showed a significant T dependence that corresponded to an *increasing* anisotropy of the in-plane scattering rate (or more precisely $1/\ell$) with increasing T, whilst the sign of the fourfold term indicated that the most intense scattering occurred near the saddles.

Subsequent ARPES measurements have revealed more information about the nature of the electronic states at different loci on the 2D FS and the corresponding self-energy corrections $\Sigma = \mathrm{Re}\,\Sigma + \mathrm{Im}\,\Sigma$ [102]. Whilst there remains some controversy regarding the precise energy, momentum and doping dependence of the self-energy, it is now well established that basal-plane anisotropy in the 'single-particle' scattering rate $\mathrm{Im}\,\Sigma$ does exist, with ill defined qp lineshapes (in the normal state) at the so-called 'anti-nodal' points near $(\pi, 0)$ coexisting with sharper qp peaks along (π, π).

Unfortunately, analysis of the energy dependence of $\mathrm{Im}\,\Sigma$ is often complicated by the onset of superconductivity, particularly since the reduction in scattering below T_c occurs not only in the inelastic, but also in the elastic channel, giving rise to additional energy-dependent terms in the self-energy [103]. For this reason, I consider here only data reported in the normal state ($T > T_c$) or for energies $\omega > \Delta$, the maximum superconducting gap value. One further advantage of focusing on the normal state is that any kink features between 50 and 100 meV, that tend to complicate the energy dependence of $\mathrm{Im}\,\Sigma$, are relatively weak there.

Early measurements on OP Bi2212 showed evidence for MFL behaviour of the normal state ARPES lineshape along the nodal direction with $\mathrm{Im}\,\Sigma \propto \omega$ [104]. More recent data however appear to suggest a dominant contribution to $\mathrm{Im}\,\Sigma$ that is *quadratic* in $|\omega|$ at low energies [105, 106], crossing over to a ω-linear dependence only above 50–100 meV. As one moves into the OD region, $\mathrm{Im}\,\Sigma$ along (π, π) becomes purely quadratic (at least up to 100 meV) [105]. Away from the nodes, it has proved difficult to determine the precise form of $\mathrm{Im}\,\Sigma(\omega)$ since the lineshapes are invariably broad and the qp states incoherent, due presumably to a strong dressing or scattering of the charge carriers in this region in **k**-space [107–109]. Kaminski *et al* showed in fact that the qp states near $(\pi, 0)$ become incoherent above a certain doping-dependent temperature which coincides with the onset of T-linear resistivity and is labelled T_{coh} in figure 2 [51]. Along the nodes, meanwhile, the qp states appear to remain coherent to much higher temperatures [106]. Finally, by carefully scanning the intermediate regions along the FS, Chang *et al* have recently uncovered a strong, highly anisotropic ω-linear contribution in OP LSCO that becomes negligible as one approaches (π, π) [110].

Extrapolating back to zero energy or to zero temperature, we find evidence for significant anisotropy in the single-particle *elastic* scattering rate or inverse mean free path (as determined by the width of the momentum distribution curve) in Bi2212 [98], Bi2201 [111] and LSCO [110, 112]. In all cases, the maximum is located near the saddles, where the density of states is largest, consistent with the picture of Abrahams and Varma for small angle scattering off out-of-plane impurities [96, 113].

Given this mounting evidence for anisotropic single-particle lifetimes in HTCs, let us now turn to consider the transport scattering rate $1/\tau_{\mathrm{tr}}$. In a 2D metal with an anisotropic $\ell(\mathbf{k})$, Ong showed that σ_{xy} is determined by the area (curl) swept out by $\ell(\mathbf{k})$ as it is traced around the FS [65] (Ong referred to this as the 'Stokes area'). Thus, anisotropy in $\ell(\mathbf{k})$, in addition to the local FS curvature, plays a fundamental role in determining both the magnitude and sign of the Hall voltage in 2D metals. Accordingly, $\cot\theta_{\mathrm{H}}(T)$ will be dominated by those regions of the FS where the curvature is greatest and/or where the qp mean free path is longest.

The Ong construction is illustrated schematically in figure 5. The solid red line in figure 5(a) represents a 2D-projected FS, similar to that shown in figure 1(b) for OD LSCO but with exaggerated negative curvature. This FS geometry gives rise to alternating sectors on the FS that have electron- and hole-like character. The purple arrows indicate the direction and length of the ℓ-vector for selected points on the FS. The angles between ℓ and **k** and between **k** and the k_x axis are labelled γ and φ respectively. As **k** moves along the FS away from the k_x axis, φ and γ increase in the same sense. At a particular **k**-point, marked by $*$, $\kappa = \mathrm{d}\gamma/\mathrm{d}\varphi$ changes sign and remains negative until φ reaches $**$. At $\varphi = \pi/2$, γ is once again equal to zero. Were $\ell(\mathbf{k})$ to be isotropic, the corresponding 'ℓ-curve' would be a circle and R_{H} would be determined simply by the FS area with a sign that reflects its location in the Brillouin zone. If ℓ is anisotropic however, as shown in figure 5(b), loops of different circulation will appear in the ℓ_x–ℓ_y plane. Ong demonstrated that σ_{xy} will then be determined by the sum of the areas enclosed by the primary (negative) and secondary (positive contribution to σ_{xy}) loops. In the simulation shown in figure 5(b), the secondary loops have the largest area and so R_{H} is of opposite sign.

In OD LSCO ($x \geqslant 0.18$), the FS encircles the Γ point in the Brillouin zone (see figure 1(b)) and has similar, if less pronounced, negative curvature to that shown in figure 5(a) [23]. The dashed line in figure 5(c) represents R_{H} calculated using the Luttinger sum rule and the isotropic-ℓ approximation, whilst the red circles are experimental R_{H}

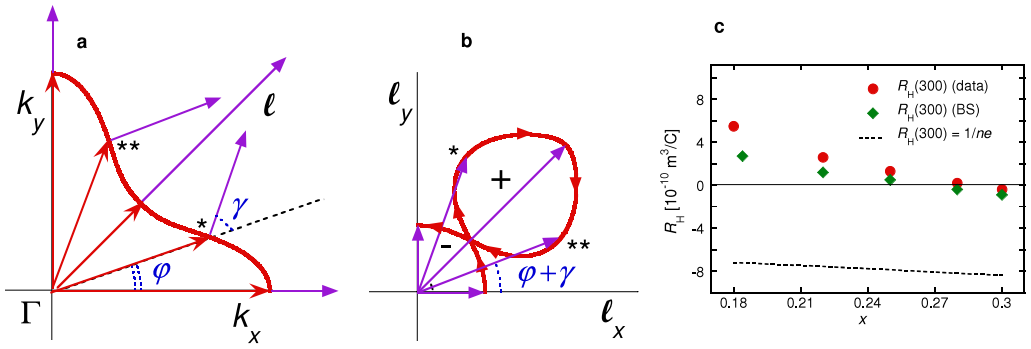

Figure 5. (a) Section of 2D Fermi surface with pronounced negative curvature. The dashed/purple (solid/red) arrows indicate the direction and length of ℓ (φ) ($k_F(\varphi)$), as explained in the text. (b) Polar plot of $\ell(\varphi+\gamma)$. The small arrows indicate the circulation of each loop and the $-/+$ signs indicate the corresponding sign of σ_{xy}. The resultant σ_{xy} is determined by the difference in the areas of the two counter-rotating loops ($\times 4$) [65]. (c) Measured (red circles, [57]) and band-derived (green diamonds) $R_H(300\ \mathrm{K})$ values in overdoped LSCO compared to the Drude value $1/ne$ (dashed line).

values at $T = 300$ K for different Sr contents [57]. For all but the highest doping level, $R_H(300\ \mathrm{K})$ is found to be of opposite sign to the expected Drude result with a magnitude that is significantly smaller than $1/ne$. At high temperatures, where scattering is sufficiently intense, one expects τ_{tr} to be isotropic within the plane. In the absence of any experimental evidence for FS reconstruction in OD LSCO [23], interpretation of these marked discrepancies in $R_H(300\ \mathrm{K})$ within a band picture must therefore imply strong in-plane anisotropy in the Fermi velocity $v_F(\varphi)$. As it happens, this is precisely what is observed experimentally. For $x = 0.30$, for example, v_F near the saddle points is three to four times smaller than along the nodal directions [112]. This anisotropy, coupled with the FS curvature, accounts almost entirely for the deviation of R_H at $T = 300$ K from its isotropic-ℓ limit, as indicated by the green triangles in figure 5(c) [99]. As x decreases, the FS retreats towards the vHs, causing the band anisotropy to grow and, correspondingly, $R_H(300\ \mathrm{K})$ to deviate even further from the isotropic-ℓ limit until eventually the vHs is crossed around $x = 0.18$ [112].

Whilst band anisotropy can appear to account for the anomalous R_H values at $T = 300$ K, it cannot explain the T dependence. For all $x \geqslant 0.18$, $R_H(T)$ is seen to become increasingly *more* positive with decreasing temperature (see figure 3(c)), implying that anisotropy in $\ell(\mathbf{k})$ becomes even more pronounced as one approaches the elastic limit. In order to account for this anomalous T dependence, additional anisotropy in the *elastic* scattering rate $\Gamma_0(\varphi)$, presumably due to static impurities, is required. In the isostructural ruthenate compound Sr_2RuO_4, the isotropic-ℓ approximation is found to be obeyed at low T [87]. La doping for Sr introduces disorder between the RuO_2 planes, and whilst it has a negligible effect on the de Haas–van Alphen frequencies (and hence the FS volume) it induces both a magnitude *and* a sign change in the zero-temperature Hall coefficient $R_H(0)$ [114]. As alluded to earlier, anisotropy in $\Gamma_0(\varphi)$ can arise due to small angle scattering off dopant impurities located between the conducting planes [96]. If d is the characteristic distance of such dopants from a plane, the electron scattering will involve only small momentum transfers $\delta k \leqslant d^{-1}$. Then, Γ_0 (φ) is proportional to δk and the local density of states, i.e. to $1/v_F(\varphi)$. A predominance of forward impurity scattering in cuprates has also been invoked to explain the weak suppression of T_c with disorder [115], and the energy and T dependence of the single-particle scattering rate Im Σ below T_c [103]. By introducing anisotropy of this form in $\Gamma_0(\varphi)$, the full T dependence of $R_H(T)$ in OD LSCO can then be qualitatively and quantitatively explained [99].

In addition to anisotropy in the elastic scattering channel, recent polar ADMR measurements in OD Tl2201 have revealed anisotropy of a similar symmetry and form in the *inelastic* scattering [17]. By incorporating basal-plane anisotropy in $\omega_c\tau$ into the ADMR analysis, Abdel-Jawad *et al* were able to extract from the full T and k dependence of ℓ_{ab} in heavily OD T2201 ($T_c = 15$ K) up to 60 K, as shown in figure 6. The T dependence of the anisotropy was attributed in full to the scattering rate, and from the resulting fits the authors were able to conclude that the scattering rate Γ contained two components, an isotropic T^2 scattering rate (presumably due to electron–electron scattering) and an anisotropic T-linear component (of unknown origin) that was maximal along (π, 0). Combining this with the elastic term, the full expression for the 'ideal' scattering rate Γ_{ideal} in OD cuprates can be written as

$$\Gamma_{ideal}(T, \varphi) = \Gamma_0(\varphi) + \Gamma_1 \cos^2(2\varphi)T + \Gamma_2 T^2 \qquad (2)$$

where $\Gamma_0(\varphi) = \beta/v_F(\varphi)$, i.e. proportional to the in-plane density of states [96]. Intriguingly, the anisotropic T-linear scattering rate has the same anisotropic form as the ω-linear contribution to Im Σ recently uncovered in OP LSCO [110]. It is also interesting to note from figure 6(c) that in Tl2201 the elastic scattering rate is almost isotropic, in marked contrast to what is seen in LSCO [110, 112]. This difference can be attributed almost entirely to their individual band structures. In Tl2201, $v_F(\varphi)$ varies by no more than 40% around the FS [19], consistent with the more rounded FS [26, 116] and its subsequent displacement away from the saddles. This level of anisotropy is one order of magnitude smaller than in LSCO. Moreover, the FS in Tl2201 does not possess negative curvature. Correspondingly, the absolute value of $R_H(0)$ in OD Tl2201 is found to be in reasonable agreement with the

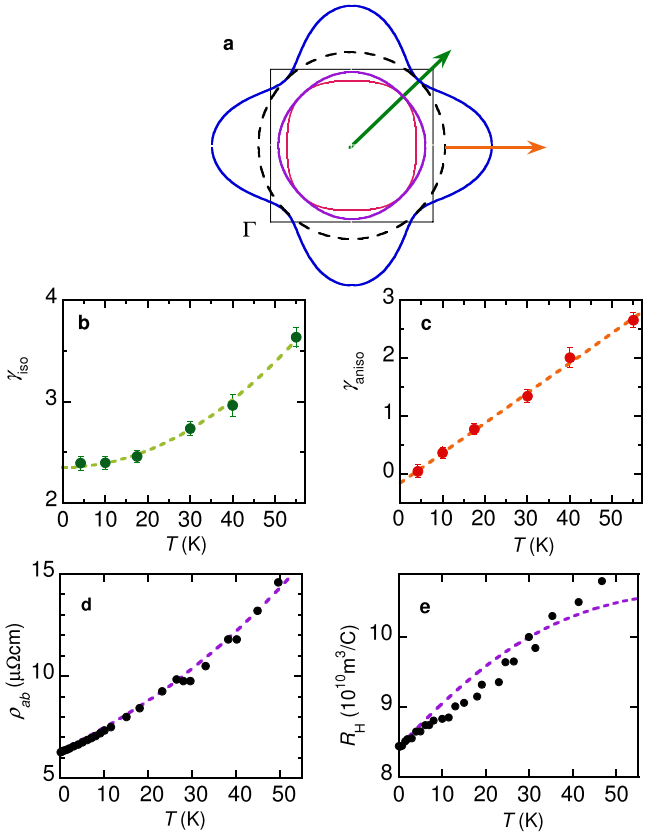

Figure 6. (a) Inner red curve: schematic 2D projection of the FS of overdoped Tl2201. Adjacent purple curve: schematic representation of the d-wave superconducting gap. Outer blue curve: geometry of $(\omega_c\tau)^{-1}(\varphi)$. Dashed black line: isotropic part of $(\omega_c\tau)^{-1}(\varphi)$. (b) T dependence of γ_{iso}, i.e. the isotropic component of $(\omega_c\tau)^{-1}(\varphi)$ and sole contribution along the 'nodal' region indicated by the green arrow in (a). The dashed curve is a fit to $A + BT^2$. (c) T dependence of γ_{aniso}, i.e. the anisotropic component of $(\omega_c\tau)^{-1}(\varphi)$ and the additional contribution that is maximal along the 'anti-nodal' direction indicated by the orange arrow in (a). The dashed curve is a fit to $C + DT$. (d) Circles: $\rho_{ab}(T)$ data for overdoped Tl2201 ($T_c = 15$ K) extracted from [49]. Dashed curve: simulation of $\rho_{ab}(T)$ from parameters extracted from the ADMR analysis. (e) Circles: $R_H(T)$ data for the same crystal [49]. Dashed curve: simulation of $R_H(T)$. Adapted with permission from *Nature Physics* **2** 821, figure 2. Copyright 2006 Macmillan Publishers Ltd.

isotropic-ℓ approximation [49] (see figure 6(e)), whilst in OD LSCO the combination of negative FS curvature and strong band anisotropy has a significant and highly non-trivial effect on $R_H(0)$. Similar detailed considerations may also be relevant to recent high-field Hall measurements on thin films of the low-T_c cuprate La-doped Bi2201, where a marked drop in $R_H(0)$ is observed near optimal doping [117]. This discontinuity in the doping dependence of $R_H(0)$ was originally associated with a marked change in the FS geometry, perhaps due to a quantum phase transition.

Significantly, the form of $\Gamma_{ideal}(T, \varphi)$ shown in equation (2) can also explain, in a quantitative and self-consistent fashion, the T dependences of $\rho_{ab}(T)$ and $R_H(T)$ in Tl2201 over the same temperature range as the ADMR measurements and, in particular, the persistence of a strong T-linear component in $\rho_{ab}(T)$ to low T reproduced in figure 6(d) [49]. Moreover, as T increases, the growth in anisotropy in $\Gamma(T, \varphi)$ is sufficient to explain the rise in $R_H(T)$, as shown in figure 6(e). Again, in heavily OD LSCO, the opposite trend seems to occur; the anisotropy starts high then gradually gets washed out with increasing temperature.

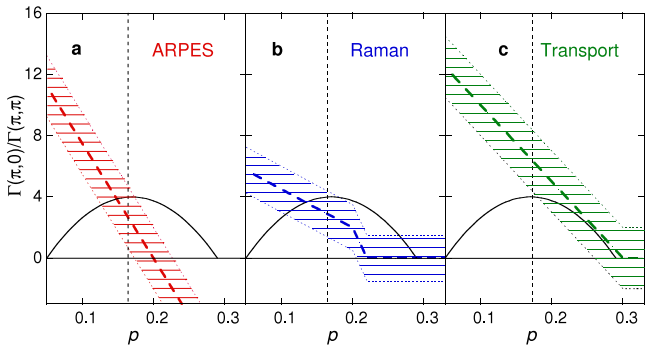

Figure 7. Schematic doping evolution of the basal-plane anisotropy of the scattering rate, defined as $\Gamma(\pi, 0)/\Gamma(\pi, \pi)$, in high-$T_c$ cuprates as revealed by (a) ARPES, (b) Raman and (c) ADMR. The black solid line represents the superconducting dome whilst the thin dashed line indicates optimal doping.

Corroborating evidence for strong basal-plane anisotropy in the *transport* scattering rate (with different T dependences) comes from Raman measurements [16]. Along the nodal direction (B_{2g} symmetry), the qp scattering rate is relatively small at all doping levels and shows metallic behaviour at all temperatures. Around $(\pi, 0)$ (B_{1g} symmetry) however, the Raman spectra are highly doping dependent, and in Bi2212 can even show non-metallic behaviour below $p = 0.15$ [16]. The ratio of the anti-nodal to nodal scattering rates $\Gamma(\pi, 0)/\Gamma(\pi, \pi)$ and their doping dependence, as inferred from ARPES [2, 116, 120], Raman [16, 118] and transport measurements [18, 88], are compared in figure 7. Whilst all three probes show a similar trend, namely an overall decline in the strength of the anisotropy with doping, there are some key differences. According to ARPES, for example, the nodal/anti-nodal quasiparticle anisotropy is seen to vanish [119, 120] or even reverse its sign [2, 116] before superconductivity is suppressed on the OD side, whilst in Raman the anisotropy collapses abruptly around $p \sim 0.20$ [16, 118]. By contrast, ADMR analysis on Tl2201 has revealed that the strength of the anisotropic scattering scales linearly with T_c, appearing to extrapolate to zero at the doping level where superconductivity vanishes [18]. The origin of these discrepancies is not clear at the time of writing. We note however that in Tl2201 ($T_c \sim 30$ K) the scattering rate deduced from ADMR [18, 79] is more than one order of magnitude smaller than the corresponding rate derived from ARPES [116], suggesting that the transport and quasiparticle lifetimes are in fact distinct.

But what of the inverse Hall angle? According to the Ong construction, $\cot\theta_H(T)$ is largely determined by the behaviour of the longest-lived quasiparticles which in hole-doped cuprates are the nodal quasiparticles near (π, π). As shown in figure 6(b), the nodal scattering rate is strictly quadratic in temperature [17]. Provided the anisotropy is sufficiently large, this nodal scattering will dominate the Hall conductivity and account for the $A + BT^2$ form of $\cot\theta_H(T)$. Given that

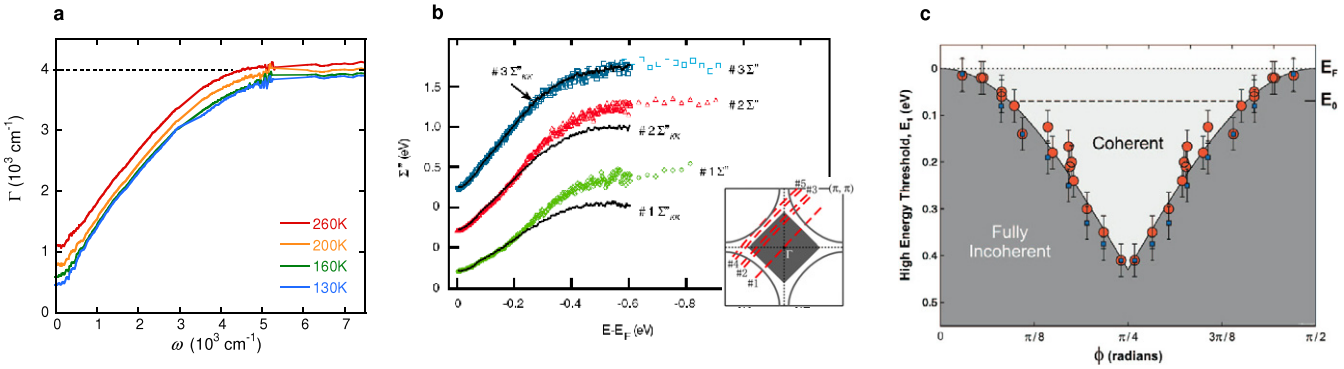

Figure 8. Scattering rate of (a) OP Bi2212 [14] and (b) OD Bi2201 [5] determined by optical conductivity and ARPES measurements respectively. In (a), the different coloured curves represent $\Gamma(\omega)$ determined for several temperatures using an extended Drude analysis of reflectivity data. The dashed line is the saturation value of $\Gamma(\omega)$. Reprinted with kind permission from [130], figure 1. Copyright 2006 by the American Physical Society. In (b), the diamonds, triangles and squares represent Im $\Sigma(\omega)$ for different cuts across the in-plane Fermi surface (shown as dashed red lines in the inset) determined from the widths of the momentum distribution curves. The solid lines labelled Σ''_{KK} are equivalent curves derived from Kramers–Kronig transformation of Re $\Sigma(\omega)$. Reprinted with kind permission from [5], figure 4b. Copyright 2007 by the American Physical Society. (c) Onset of saturation as a function of azimuthal angle in OP LSCO. 0 and $\pi/2$ refer to those regions closest to the saddle points [8]. Reprinted with kind permission from [8], figure 3. Copyright 2007 by the American Physical Society.

Im $\Sigma \propto \omega^2$ along the nodes [105, 106], this form of scattering appears to be purely electronic in origin. Whilst the broad energy range over which this quadratic dependence persists may appear anomalous, similar behaviour is observed in other correlated oxides such as Sr_2RuO_4 [121], Sr_2RhO_4 [122] and $PrBa_2Cu_4O_8$ [123]. Finally, the reduction in the strength of the anisotropic scattering with doping, highlighted in figure 7, can offer an explanation for the softening of the exponent α in the T dependence of $\cot\theta_H(T)$ $(=A + BT^\alpha)$ in both Bi2201 and Bi2212 (from 2 to 1.65) as one moves across the phase diagram [75, 76]; as the anisotropy in $\ell(\mathbf{k})$ is reduced, regions of the FS away from the nodes, where $\ell(\mathbf{k})$ is larger and the T dependence is weaker than T^2, begin to contribute to σ_{xy} and thus to $\cot\theta_H(T)$ [88].

8. Scattering rate saturation

In recent years, the energy scale over which the qp excitation spectrum can be probed by optical and photoemission spectroscopies has increased markedly, allowing access to the full spectral response up to the bare (or renormalized) bandwidth W. One striking feature of the high energy response has been the tendency of the single-particle or particle–particle scattering rate towards saturation. Such behaviour is exemplified by recent state-of-the-art optical reflectivity data on OP $Bi_2Sr_2Ca_{0.92}Y_{0.08}Cu_2O_8$ (Y-Bi2212) [14], analysed using an 'extended' or 'generalized' Drude model that assumes a single Drude component for $\omega < W$ but with a scattering rate $\Gamma(T, \omega)$ and coupling constant $\lambda(T, \omega)$ that are frequency dependent.

As shown in figure 8(a), $\Gamma(T, \omega)$ initially grows linearly with frequency but above 3000 cm^{-1} it starts to deviate from linearity, tending to a constant value $\Gamma_{max} \sim 4000$ cm^{-1} ($\sim$0.5 eV). At first sight, such 'saturation' in $\Gamma(T, \omega)$ appears suggestive of strong coupling to bosons, though the high frequency at which saturation sets in ($\sim$4000 cm^{-1}) implies that these are not phonons [124]. Norman and Chubukov [125] recently argued that a model based on coupling to a broad spectrum of spin fluctuations, extending out to 0.3 eV, captures most of the essential features of the data in [14], although a gapped MFL model was also found to work reasonably well. Similarly, Hwang *et al* extracted Eliashberg-type functions from optical conductivity data on UD YBCO [126] and OP LSCO [127] and showed them to be consistent with the spectrum of spin fluctuations obtained independently from INS measurements [128, 129]. In each case, however, neglect of the basal-plane anisotropy in $\Gamma(T, \omega)$ in the modelling may have compromised the analysis significantly [130].

One aspect of the data in figure 8(a) that is at odds with the standard picture of electron–boson coupling is its T dependence. According to the original Allen formalism [124, 131], saturation of $\Gamma(\omega)$ sets in at progressively higher frequencies as T is raised, more so still if the bosonic response were to broaden and shift to higher frequencies, as is expected if the strongest coupling is to antiferromagnetic spin fluctuations [127]. The data do *not* show this tendency; if anything, $\Gamma(\omega)$ saturates at a *lower* frequency as T increases. This counter-trend in $\Gamma(T, \omega)$ is seen particularly clearly in the optical response of UD $Ca_{2-x}Na_xCuO_2Cl_2$ [132]. Hwang *et al* proposed a way around this problem by combining their Eliashberg-type analysis with a frequency-dependent density of states that served to mimic the pseudogap in UD YBCO [126], though yet again no account was made of its angular dependence.

Saturation is also seen in the single-particle scattering rate Im Σ, an example of which is shown in figure 8(b) for OD Bi2201 [5]. As with the optical scattering rate, saturation does not set in until extremely high energies, of the order of 0.5 eV (4000 cm^{-1}), and attains values of the order of 1 eV ($\sim W$), that suggests the development of incoherent excitations [5]. Similar observations have now been reported for OP Bi2212 [6] and OP LSCO [8]. Notably, in OP LSCO, Im $\Sigma(\omega)$ appears to saturate at different points on the FS at different energies, in line with the strong basal-plane anisotropy in Im $\Sigma(\omega, \varphi)$ [8, 110]. As shown in figure 8(c), Im $\Sigma(\omega)$ near $(\pi, 0)$ is found to saturate close to the Fermi level, whilst along the

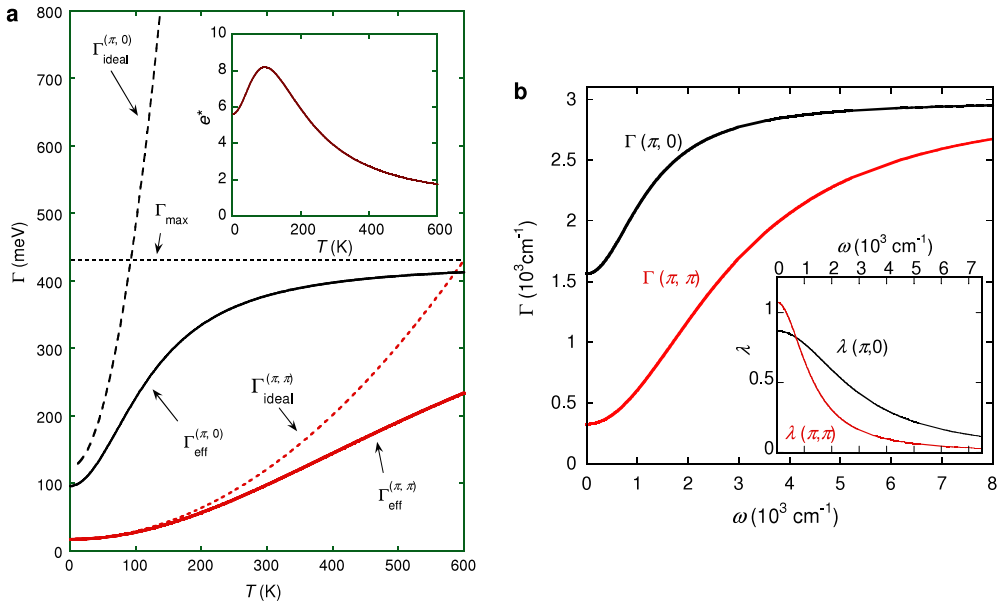

Figure 9. Left panel: T dependence of the ideal and effective scattering rates for $(\pi, 0)$ and (π, π) for OP Tl2201. Inset: T dependence of the effective anisotropy $e^* = \Gamma_{\rm eff}^{(\pi,0)}/\Gamma_{\rm eff}^{(\pi,\pi)} - 1$ for the same parametrization. Adapted from [88]. Copyright 2003 by Springer. Right panel: $\Gamma_{\rm eff}(\omega)$ along (π, π) and $(\pi, 0)$ at $T = 200$ K for OP Y-Bi2212. Inset: corresponding $\lambda_{\rm eff}(\omega)$ for the same two orientations, obtained via the appropriate Kramers–Kronig transformation. Reprinted with kind permission from [130], figure 2. Copyright 2006 by the American Physical Society.

nodes, coherence survives up to 0.4 eV. This is reminiscent of the evolution of Im Σ with temperature in Bi2212 where anti-nodal states become incoherent above T_c [51], whilst those along the diagonals remain coherent up to much higher temperatures [105, 106].

An alternative way to interpret this coherent/incoherent crossover and the onset of saturation in $\Gamma(\omega)$ is to invoke the Mott–Ioffe–Regel (MIR) limit for coherent charge propagation. The MIR criterion states that the electron mean free path ℓ has a lower limit of the order of the interatomic spacing a (or, to put it another way, Γ can never exceed the bare bandwidth W). Beyond this point, the concept of carrier velocity is lost and all coherent quasiparticle motion vanishes. Such a threshold is seen, for example, in metals exhibiting resistivity saturation, where the saturation value is found to be consistent with $\ell = a$ [133, 134]. For Y-Bi2212, one can estimate $\Gamma_{\rm max} = \langle v_{\rm F}\rangle/a \sim 4500$ cm^{-1} using parameters independently extracted from both optics [14] and ARPES [135]. Comparison with figure 8(a) suggests that the saturation value of $\Gamma(T, \omega)$ is indeed comparable with the MIR limit as defined.

Puzzlingly, saturation in $\Gamma(\omega)$ at or near the MIR limit does not appear to be manifest in the dc transport properties where, in OP LSCO for example, $\rho_{ab}(T)$ grows approximately linearly with T up to 1000 K, reaching values of the order 1–10 mΩ cm, that correspond to $\ell \ll a$ [74]. Detailed analysis of optical conductivity data in cuprates and in other so-called 'bad metals', however, has shown that as the MIR limit is attained loss of coherence is identified by a suppression of low-frequency spectral weight and the development of a non-Drude optical response [134]. The lost weight is transferred to energies $\omega > W$ ($\sim$1 eV) and the optical sum rule is only fulfilled at much higher energies of 2–3 eV [136, 137]. This collapse of the zero-frequency collective mode implies that continuation of the positive slope of $\rho_{ab}(T)$ well into the incoherent regime has nothing to do with an unbounded escalation of the scattering rate. It also brings into question association of saturation in $\Gamma(\omega)$ with bosonic mode coupling, since there one might expect the scattering rate to continue to grow and the Drude response continue to broaden. This is not what is observed.

So how does saturation in $\Gamma(\omega)$ at high energies impact on the dc transport properties? In metals that exhibit resistivity saturation, the form of the resistivity is extremely well captured by the so-called 'parallel-resistor' model [138], $1/\rho(T) = 1/\rho_{\rm ideal}(T) + 1/\rho_{\rm max}$, where $\rho_{\rm ideal}$ is the ideal resistivity (i.e. in the absence of saturation, typically the Bloch–Grüneisen resistivity), that is shunted by a large saturation resistivity $\rho_{\rm max}$ corresponding to $\ell = a$. Whilst the origin of this behaviour is still not understood, one can readily assume that the parallel-resistor form of the resistivity in such metals reflects that of the scattering rate, which one can easily modify to include anisotropy [88] by defining an 'effective' scattering rate $\Gamma_{\rm eff}$ as

$$1/\Gamma_{\rm eff}(T, \varphi) = 1/\Gamma_{\rm ideal}(T, \varphi) + 1/\Gamma_{\rm max}. \qquad (3)$$

Note that this formula implies scattering rates adding in parallel rather than different conduction channels. Use of equation (3) acknowledges that the MIR limit is manifest at all temperatures and, by extension, all energies below the bandwidth, hence its potential impact on the dc transport. In optimally and overdoped HTCs, $1/\Gamma_{\rm ideal}(T, \varphi)$ is given by equation (2). A schematic demonstration of the role of equation (3) is shown in figure 9(a), where the T dependences of $\Gamma_{\rm eff}(T, \varphi)$ for the two key momentum directions $(\pi, 0)$ and (π, π) are plotted. For illustrative purposes, $\Gamma_1 = 0$ and the

anisotropy parameters used in this simulation are those applied originally to OP Tl2201 to produce a T-linear resistivity, an inverse Hall angle $\cot\theta_H \sim A + BT^2$ and a modified Kohler's rule of the correct magnitude [88]. Along $(\pi, 0)$, $\Gamma_{ideal}(T)$ reaches Γ_{max} at $T_c \sim$ 90 K, at which point the anti-nodal quasiparticles start to lose coherence. Due to the presence of the 'shunt' Γ_{max}, however, $\Gamma_{eff}(T)$ is always smaller than $\Gamma_{ideal}(T)$ and approaches saturation much more gradually. For the quasiparticles at (π, π), on the other hand, $\Gamma_{ideal}(T)$ reaches Γ_{max} at a much higher temperature ($T \sim 600$ K). Hence, at the nodal points, well defined coherent quasiparticles exist at all relevant temperatures. Note that $\Gamma_{eff}(T)$ at (π, π) is quasilinear over a wide temperature range. Within this model, the onset of T-linear resistivity above T_{coh} (see figure 2) coincides with the temperature at which $\Gamma_{ideal}^{(\pi,0)}$ exceeds Γ_{max}, in excellent agreement with what has been inferred from ARPES measurements on OP Bi2212 [51, 105, 106].

Correspondingly, the 'effective' anisotropy factor e^* $(=\Gamma_{eff}^{(\pi,0)}/\Gamma_{eff}^{(\pi,\pi)} - 1)$ also reaches a maximum value at this temperature (see inset to figure 9(a)). The overall effect is a transport scattering rate $\Gamma_{eff}(T, \varphi)$ whose anisotropy initially grows with increasing T but then gradually becomes more isotropic at higher temperatures as the scattering rate at different regions of the FS tends towards saturation. In this way, the T dependence of $e^*(T)$ (figure 9(a)) mimics that of the Hall coefficient $R_H(T)$ in HTC; another example of saturation playing a key role in a dc transport property. Finally, with increasing doping (away from optimal doping), the relative anisotropy decreases gradually to zero (figure 7) as one approaches the non-superconducting normal metallic region [18, 88, 139], leading to a lessening of the T dependence of $R_H(T)$ as observed experimentally [140].

It is relatively straightforward to extend this idea into the frequency domain [130]. Figure 9(b) shows the evaluated frequency-dependent scattering rate $\Gamma_{eff}(\omega)$ along (π, π) (red line) and $(\pi, 0)$ (black line) used to fit the optical conductivity data on Y-Bi2212 at $T = 200$ K [14]. The inset shows the corresponding mass enhancement factors $\lambda_{eff}(\omega)$ obtained via the appropriate Kramers–Kronig transformation. (Again for simplicity, $\Gamma_1 = 0$ here.) The anisotropy in λ_{eff} is considerably weaker than in Γ_{eff}, highlighting the surprisingly large effect of saturation on the mass enhancement, even at the dc limit. Indeed, suppression of $\lambda(0)$, the zero-frequency coupling constant, becomes stronger as $\Gamma_{ideal}(\omega = 0)$ approaches Γ_{max} [141]: a feature that may help to explain why mass enhancement in HTCs does not diverge near the Mott transition.

As described above, this dichotomy in the nodal and anti-nodal qp states has been intimated by a variety of different experiments, including ARPES [8, 51, 106], Raman [118], Hall effect [142] and even STM [3]. Whilst it appears difficult to differentiate between total incoherence (suppression of spectral weight) and saturation of the scattering rate at the MIR limit, the inclusion of a maximal scattering rate in the analysis appears particularly instructive, and, phenomenologically at least, it can help to explain a wide range of physical observables. Its overall effect is to reduce the anisotropy between the nodal and anti-nodal states, thereby masking to some extent the intrinsic anisotropy created by whatever physical process is responsible. Moreover, by invoking the 'parallel-resistor' model, the saturation of the T- or ω-dependent scattering rate at the MIR limit is seen to influence the transport behaviour in cuprates over a very wide energy scale, even down to the dc limit, and to acknowledge its presence may yet turn out to be a key step in the development of a coherent description of the charge dynamics.

9. Discussion and conclusions

In this review article, I have highlighted a number of recent experimental results which shed new light on the cuprate transport problem and have identified those ingredients I believe are necessary for a complete phenomenological description of the anomalous normal state transport properties of optimally doped and overdoped high-T_c cuprates. These ingredients are summarized in equations (1)–(3) in the main body of the article: namely, the tight-binding band structure, basal-plane anisotropy in both the elastic and the inelastic T-linear scattering channels, an isotropic electron–electron scattering term and, finally, saturation of all scattering at or near the Mott–Ioffe–Regel limit.

In order to investigate to what extent this phenomenology captures the overall physical behaviour in HTCs, I show here a simple one-parameter scaling of the doping evolution of $\rho_{ab}(T, p)$ and $R_H(T, p)$ in Tl2201. In this simulation, the FS parameters are fixed by the ADMR measurements on OD Tl2201 ($T_c = 15$ K; see figure 2(c) [18]) and scaled for each p-value by the empirical relation $T_c/T_c^{max} = 1 - 82.6(p - 0.16)^2$ with $T_c^{max} = 92$ K [143]. Secondly, $\Gamma_{ideal}(\varphi, T)$ is expressed using equation (2) with Γ_0 and Γ_2 assumed to be doping (and k) independent and fixed by the values determined for the $T_c = 15$ K sample [18]. Hence the only parameter that is allowed to vary is the strength of the anisotropic T-linear term $\Gamma_1 = \Gamma_1(15\,\text{K}) \times T_c(p)/15$. The anticipated return to isotropic scattering at high T is simulated by inclusion (in parallel) of a maximum scattering rate Γ_{max} $(=\langle v_F \rangle/a)$ in accord with the MIR limit (equation (3)). The corresponding $\Gamma_{eff}(T, \varphi)$ is then inserted, along with the FS parameters, into the appropriate expressions for ρ_{ab} and R_H derived using the Jones–Zener form of the Boltzmann equation for a quasi-2D FS [88].

The resultant simulations for $R_H(T, p)$ and $\rho_{ab}(T, p)$ are presented in figure 10 for $T_c = 10$, 25, 50 and 80 K. Despite there being no free parameters in the modelling (Γ_1 is essentially fixed by T_c), the $R_H(T)$ plots show good qualitative agreement with the published data (solid symbols, [45, 79, 140]). The p dependence of $\rho_{ab}(T)$ $(=\rho_0 + \nu T^n)$ is also found to be reasonably consistent with experiment, with the exponent n evolving smoothly from two at the SC/non-SC boundary towards unity as one approaches optimal doping [140]. The fact that our simulations capture the marked ($\times 2$) increase in the magnitude of R_H (and ρ_{ab}) for what are relatively small ($\sim$5%) changes in carrier concentration suggests that anisotropic scattering is indeed a dominant contributor to the T and p dependence of R_H and ρ_{ab} across the OD regime, whilst the *monotonic* variation of $R_H(T, p)$ argues against any sign reversal of the scattering rate anisotropy near $p = 0.2$ as inferred from ARPES [2, 116]. Discrepancies

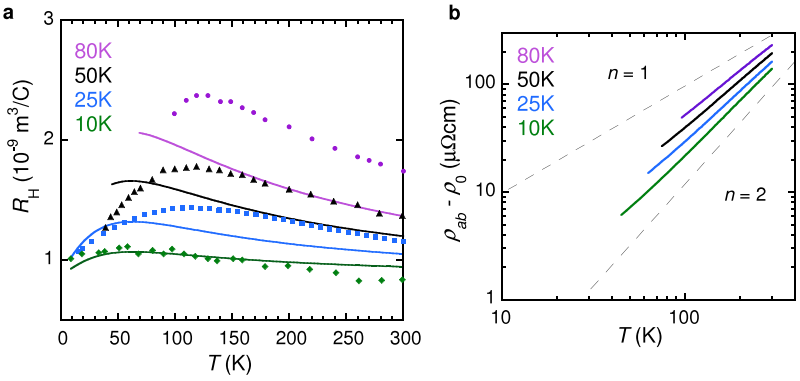

Figure 10. (a) $R_H(T)$ simulations for Tl2201 with T_c values of 10, 25, 50 and 80 K (solid lines) together with published data for 10 K (green diamonds [45]), 25 K (blue squares [79]) and 50 K (black triangles [45]) single crystals plus polycrystalline data for $T_c = 81$ K (purple circles, [140]). (b) Simulation of $\rho_{ab}(T) - \rho_{ab}(T = 0)$ (on a log–log scale) using the same parametrization. Adapted with kind permission from [18], figure 3. Copyright 2007 by the American Physical Society.

between the fitting and the model seem to grow stronger as one progressively lowers the doping. These might be attributable to the gradual emergence of current vertex corrections (also known as 'backflow') that act to modify the direction of the effective quasiparticle velocity (and thus the direction of the total current), leading to exaggeration of the curvature in $\ell(k)$ and hence a stronger renormalization of R_H [144]. Since interlayer transport in cuprates is believed to be determined by a product of *single-particle* spectral functions on adjacent planes [145], it is possible that parameters obtained by ADMR, an *interlayer* tunnelling measurement, do not include these corrections.

Such details notwithstanding, the overall experimental situation does appear to support models in which anisotropic T-linear scattering, in conjunction with the Fermi surface curvature and band anisotropy [65], is primarily responsible for the T dependence of $\rho_{ab}(T)$ and $R_H(T)$. The origin of the anisotropic scattering is not known at present. Interactions with a bosonic mode are one obvious candidate, though given the strong angle and doping dependence presumably not phonons. Whilst phonons can give rise to anisotropic scattering, the behaviour of $\Gamma(\omega)$, extracted from extended Drude analysis of the in-plane optical conductivity, as described above, is inconsistent with an electron–boson scattering response due to phonons [14]. Moreover, it has proved problematic to explain the quadratic T dependence of the inverse Hall angle $\cot\theta_H(T)$ in a scenario based solely on electron–phonon scattering. More likely candidates include spin [89, 90], charge (stripe) [91] or d-wave pairing fluctuations [92], all of which disappear with superconductivity on the OD side [92, 146, 147]. The preservation of the T-linear scattering rate to low T, however, would seem to imply a vanishingly small energy scale for such fluctuations, characteristic of proximity to a quantum critical point. This feature of the scattering is perhaps more consistent with MFL phenomenology, particularly since a similar ω-linear dependence has also been seen in $\mathrm{Im}\,\Sigma$ (in LSCO) [110]. Its vanishing at the nodes and the coexistence of a ubiquitous T^2 dependence however represent significant challenges to this scenario that have yet to be addressed. In the original two-lifetime picture, meanwhile, no basal-plane anisotropy has ever been considered. More recently, the transport scattering rate close to a 2D Pomeranchuk instability was shown to have a form identical to that observed in OD Tl2201 [93]. In such a scenario, however, the magnitude of the anisotropy should grow, rather than diminish, with doping as the vHs is approached on the OD side. Finally, real-space (correlated) electronic inhomogeneity [3] cannot be excluded as a possible origin of the **k**-space anisotropy, though as yet no measurements have been performed on heavily OD non-SC cuprates to establish any possible link between inhomogeneity and superconductivity. Thus, at the time of writing, it appears that none of the existing models are wholly consistent with the form derived for $\ell(\mathbf{k})$, and clearly more theoretical input is required.

Extension of the analysis of ARPES and optical conductivity measurements to high energies has revealed the tendency towards saturation in both the single-particle and the particle–particle scattering rates with an onset that occurs at different temperatures and/or energies depending on the location in **k** space. Saturation generally masks the intrinsic nature of $\Gamma(\omega)$ in many of the physical properties that are measured and this may explain why it has taken the community so long to reach a consensus on the various interactions and scattering mechanisms that influence the self-energy of the in-plane anti-nodal quasiparticles in cuprates, and which ultimately may drive high temperature superconductivity. Measurements that focused on the heavily overdoped region of the phase diagram, where saturation is less of an issue, have been able to reveal for the first time the precise form of the additional scattering rate, that is maximal at the anti-nodes and increases in intensity as the doping level is reduced [17, 18]. What intrinsic form this anisotropic scattering takes in the underdoped region may never be known, particularly since the pseudogap itself may act to suppress scattering in a highly non-trivial and anisotropic fashion and require a detailed, self-consistent, microscopic formalism to address. On the experimental side, more systematic k-dependent transport and spectroscopic studies in this region of the phase diagram would be highly beneficial. It would also be helpful to search for universality amongst the different classes of HTC compounds. Although similar phenomenology in the transport properties has been reported in Tl2201, Bi2212 and Bi2201,

and differences in $R_H(T)$ in LSCO can be explained largely by differences in its fermiology, there are still outstanding issues, for example the very strong T dependence of $R_H(T)$ in YBCO, that need to be addressed.

But I do not wish to end on a pessimistic note. Indeed, as chronicled throughout this review, the last few years have witnessed remarkable progress as experimentalists have developed more guile and delved deeper into the mysteries of HTC. Almost in celebration of its coming of age, very recent measurements involving pulsed high magnetic fields have uncovered a wealth of remarkable and previously unforeseen features of the low T transport behaviour of UD YBCO, such as quantum oscillations [28, 148, 149], negative Hall coefficient [150] and metallic T^2 resistivity [151, 152], all of which have sparked renewed debate within the community. These important developments have provided new insight into the nature of the fermiology and qp states in underdoped cuprates and will no doubt feature strongly in future interpretations of the normal state transport properties of HTCs. I look forward to such developments with interest.

Acknowledgments

The author would like to acknowledge M Abdel-Jawad, J G Analytis, L Balicas, A F Bangura, A Carrington, R A Cooper, M M J French and A Narduzzo for contributing to this work and helping the author to formulate many of the ideas presented. This work was supported by EPSRC (UK).

References

[1] Cho A 2006 *Science* **314** 1072
[2] Zhou X J *et al* 2004 *Phys. Rev. Lett.* **92** 187001
[3] McElroy K, Lee D-H, Hoffman J E, Lang K M, Lee J, Hudson E W, Eisaki H, Uchida S and Davis J C 2005 *Phys. Rev. Lett.* **94** 197005
[4] Graf J *et al* 2007 *Phys. Rev. Lett.* **98** 067004
[5] Xie B P *et al* 2007 *Phys. Rev. Lett.* **98** 147001
[6] Valla T, Kidd T E, Pan Z-H, Fedorov A V, Yin W-G, Gu G D and Johnson P D 2007 *Phys. Rev. Lett.* **99** 167003
[7] Meevasana W *et al* 2007 *Phys. Rev.* B **75** 174506
[8] Chang J *et al* 2007 *Phys. Rev.* B **75** 224508
[9] Hayden S M *et al* 2004 *Nature* **429** 531
[10] Tranquada J M *et al* 2004 *Nature* **429** 534
[11] Molegraaf H J A, Presura C, van der Marel D, Kes P H and Li M 2002 *Science* **295** 2239
[12] Santander-Syro A F, Lobo R P S M, Bontemps N, Konstantinovic Z, Li Z Z and Raffy H 2003 *Europhys. Lett.* **62** 568
[13] Boris A V, Kovaleva N N, Dolgov O V, Holden T, Lin C T, Keimer B and Bernhard C 2004 *Science* **304** 708
[14] van der Marel D, Molegraaf H J A, Zaanen J, Nussinov Z, Carbone F, Damascelli A, Eisaki H, Greven M, Kes P H and Li M 2003 *Nature* **425** 271
[15] Hwang J, Nicol E J, Timusk T, Knigavko A and Carbotte J P 2007 *Phys. Rev. Lett.* **98** 207002
[16] Devereaux T P and Hackl R 2007 *Rev. Mod. Phys.* **79** 175
[17] Abdel-Jawad M, Kennett M P, Balicas L, Carrington A, Mackenzie A P, McKenzie R H and Hussey N E 2006 *Nat. Phys.* **2** 821
[18] Abdel-Jawad M, Analytis J G, Balicas L, Carrington A, Charmant J P A, French M M J, Mackenzie A P and Hussey N E 2007 *Phys. Rev. Lett.* **99** 107002
[19] Analytis J G, Abdel-Jawad M, Balicas L, French M M J and Hussey N E 2007 *Phys. Rev.* B **76** 104523
[20] Zaanen J *et al* 2006 *Nat. Phys.* **2** 138
[21] Pavarini E, Dasgupta I, Saha-Dasgupta T, Jepsen O and Andersen O K 2001 *Phys. Rev. Lett.* **87** 047003
[22] Tanaka K *et al* 2004 *Phys. Rev.* B **70** 092503
[23] Yoshida T *et al* 2006 *Phys. Rev.* B **74** 224510
[24] Kaminski A, Rosenkranz S, Fretwell H M, Norman M R, Randeria M, Campuzano J C, Park J-M, Li Z Z and Raffy H 2006 *Phys. Rev.* B **73** 174511
[25] For a review see: Zhou X J *et al* 2006 *Treatise on High Temperature Superconductivity* ed J R Schrieffer (Amsterdam: Springer)
[26] Hussey N E, Abdel-Jawad M, Carrington A, Mackenzie A P and Balicas L 2003 *Nature* **425** 814
[27] Kanigel A *et al* 2006 *Nat. Phys.* **2** 447
[28] Doiron-Leyraud N *et al* 2007 *Nature* **447** 565
[29] Timusk T and Statt B 1999 *Rep. Prog. Phys.* **62** 61
[30] Bucher B, Steiner P, Karpinski J, Kaldis E and Wachter P 1993 *Phys. Rev. Lett.* **70** 2012
[31] Ito T, Takenaka K and Uchida S 1993 *Phys. Rev. Lett.* **70** 3995
[32] Hussey N E, Nozawa K, Takagi H, Adachi S and Tanabe K 1997 *Phys. Rev.* B **56** R11423
[33] Nakano T, Momono N, Oda M and Ido M 1998 *J. Phys. Soc. Japan* **67** 2622
[34] Watanabe T, Fujii T and Matsuda A 1997 *Phys. Rev. Lett.* **79** 2113
[35] Ando Y, Boebinger G S, Passner A, Kimura T and Kishio K 1995 *Phys. Rev. Lett.* **75** 4662
[36] Boebinger G S *et al* 1996 *Phys. Rev. Lett.* **77** 5417
[37] Ono S, Ando Y, Murayama T, Balakirev F F, Betts J B and Boebinger G S 2000 *Phys. Rev. Lett.* **85** 638
[38] Proust C *et al* 2008 unpublished
[39] Ando Y, Komiya S, Segawa K, Ono S and Kurita Y 2004 *Phys. Rev. Lett.* **93** 267001
[40] Hussey N E, Takagi H, Iye Y, Tajima S, Rykov A I and Yoshida K 2000 *Phys. Rev.* B **61** R6475
[41] Hussey N E, Cooper J R, Kodama Y and Nishihara Y 1998 *Phys. Rev.* B **58** R611
[42] Ono S and Ando Y 2003 *Phys. Rev.* B **67** 104512
[43] Giura M, Fastampa R, Sarti S and Silva E 2003 *Phys. Rev.* B **68** 134515
[44] Tyler A W and Mackenzie A P 1997 *Physica* C **282–287** 1185
[45] Manako T, Kubo Y and Shimakawa Y 1992 *Phys. Rev.* B **46** 11019
[46] Homes C C *et al* 2004 *Nature* **430** 539
[47] Yoshida K, Rykov A I, Tajima S and Terasaki I 1999 *Phys. Rev.* B **60** R15035
[48] Custers J *et al* 2003 *Nature* **424** 524
[49] Mackenzie A P, Julian S R, Sinclair D C and Lin C T 1996 *Phys. Rev.* B **53** 5848
[50] Naqib S H, Cooper J R, Tallon J L and Panagopoulos C 2003 *Physica* C **387** 365
[51] Kaminski A, Rosenkranz S, Fretwell H M, Li Z Z, Raffy H, Randeria M, Norman M R and Campuzano J C 2003 *Phys. Rev. Lett.* **90** 207003
[52] Nakamae S, Behnia K, Yates S J C, Mangkorntong N, Nohara M, Takagi H and Hussey N E 2003 *Phys. Rev.* B **68** 100502
[53] Dagan Y and Greene R L 2007 *Phys. Rev.* B **76** 024506
[54] Fournier P, Mohanty P, Maiser E, Darzens S, Venkatesan T, Lobb C J, Czjzek G, Webb R A and Greene R L 1998 *Phys. Rev. Lett.* **81** 4720
[55] Dagan Y, Qazilbash M M, Hill C P, Kulkarni V N and Greene R L 2004 *Phys. Rev. Lett.* **92** 167001
[56] Gauthier J, Gagné S, Renaud J, Gosselin M-È, Fournier P and Richard P 2007 *Phys. Rev.* B **75** 024424
[57] Hwang H Y *et al* 1994 *Phys. Rev. Lett.* **72** 2636

[58] Nishikawa T, Takeda J and Sato M 1994 *J. Phys. Soc. Japan* **63** 1441
[59] Ong N P, Wang Z Z, Clayhold J, Tarascon J M, Greene L H and McKinnon W R 1987 *Phys. Rev.* B **35** 8807
[60] Takagi H, Ido T, Ishibashi S, Uota M, Uchida S and Tokura Y 1989 *Phys. Rev.* B **40** 2254
[61] Ando Y, Komiya S, Segawa K, Ono S and Kurita Y 2004 *Phys. Rev. Lett.* **92** 197001
[62] Ino A *et al* 2002 *Phys. Rev.* B **65** 094504
[63] Yoshida T *et al* 2003 *Phys. Rev. Lett.* **91** 027001
[64] Tsukada I and Ono S 2006 *Phys. Rev.* B **74** 134508
[65] Ong N P 1991 *Phys. Rev.* B **43** 193
[66] Ono S and Ando Y 2007 *Phys. Rev.* B **75** 024515
[67] Uchida S *et al* 1991 *Phys. Rev.* B **43** 7942
[68] Wang Z Z, Chien T R, Ong N P, Tarascon J M and Wang E 1991 *Phys. Rev.* B **43** 3020
[69] Li P, Balakirev F F and Greene R L 2007 *Phys. Rev. Lett.* **99** 047003
[70] Matsui H, Terashima K, Sato T, Takahashi T, Wang S-C, Yang H-B, Ding H, Uefuji T and Yamada K 2005 *Phys. Rev. Lett.* **94** 047005
[71] Lin J and Millis A J 2005 *Phys. Rev.* B **72** 214506
[72] Armitage N P *et al* 2002 *Phys. Rev. Lett.* **88** 257001
[73] Chien T R, Wang Z Z and Ong N P 1991 *Phys. Rev. Lett.* **67** 2088
[74] Gurvitch M and Fiory A T 1987 *Phys. Rev. Lett.* **59** 1337
[75] Ando Y and Murayama T 1999 *Phys. Rev.* B **60** R6991
[76] Konstantinovic Z, Li Z Z and Raffy H 2000 *Phys. Rev.* B **62** R11989
[77] Luo N and Miley G H 2002 *Physica* C **371** 259
[78] Harris J M, Yan Y F, Matl P, Ong N P, Anderson P W, Kimura T and Kitazawa K 1995 *Phys. Rev. Lett.* **75** 1391
[79] Hussey N E *et al* 1996 *Phys. Rev. Lett.* **76** 122
[80] Kimura T *et al* 1996 *Phys. Rev.* B **53** 8733
[81] Latyshev Y I, Laborde O and Monceau P 1995 *Europhys. Lett.* **29** 495
[82] Leridon B, Défossez A, Dupont J, Lesueur J and Contour J P 2001 *Phys. Rev. Lett.* **87** 197007
[83] Larkin A I and Varlamov A A 2002 *The Physics of Superconductors* (*Conventional and High-Tc Superconductors* vol I) ed K-H Bennemann and J B Ketterson (Tokyo: Springer)
[84] Alexandrov A S, Kabanov V V and Mott N F 1996 *Phys. Rev. Lett.* **77** 4796
[85] Bok J and Bouvier J 2004 *Physica* C **403** 263
[86] Cooper J R and Loram J W 1996 *J. Physique* I **6** 2237
[87] Mackenzie A P, Hussey N E, Diver A J, Julian S R, Maeno Y, Nishizaki S and Fujita T 1996 *Phys. Rev.* B **54** 7425
[88] Hussey N E 2003 *Eur. Phys. J.* B **31** 495
[89] Carrington A, Mackenzie A P, Lin C T and Cooper J R 1992 *Phys. Rev. Lett.* **69** 2855
[90] Monthoux P and Pines D 1992 *Phys. Rev.* B **49** 4261
[91] Castellani C, di Castro C and Grilli M 1995 *Phys. Rev. Lett.* **75** 4650
[92] Ioffe L B and Millis A J 1998 *Phys. Rev.* B **58** 11631
[93] Dell'Anna L and Metzner W 2007 *Phys. Rev. Lett.* **98** 136402
[94] Anderson P W 1991 *Phys. Rev. Lett.* **67** 2092
[95] Varma C M, Littlewood P B, Schmitt-Rink S, Abrahams E and Ruckenstein A E 1989 *Phys. Rev. Lett.* **63** 1996
[96] Varma C M and Abrahams E 2001 *Phys. Rev. Lett.* **86** 4652
[97] Grayson M, Rigal L B, Schmadel D C, Drew H D and Kung P-J 2002 *Phys. Rev. Lett.* **89** 037003
[98] Valla T, Fedorov A V, Johnson P D, Li Q, Gu G D and Koshizuka N 2000 *Phys. Rev. Lett.* **85** 828
[99] Narduzzo A *et al* 2007 *Preprint* cond-mat/0707.4601 v1
[100] Hlubina R 2001 *Phys. Rev.* B **64** 132508
[101] Carter E and Schofield A J 2002 *Phys. Rev.* B **66** 241102
[102] Damascelli A, Hussain Z and Shen Z-X 2003 *Rev. Mod. Phys.* **75** 473
[103] Zhu L, Hirschfeld P J and Scalapino D J 2004 *Phys. Rev.* B **70** 214503
[104] Valla T, Fedorov A V, Johnson P D, Wells B O, Hulbert S L, Li Q, Gu G D and Koshizuka N 1999 *Science* **285** 2110
[105] Kordyuk A A *et al* 2004 *Phys. Rev. Lett.* **92** 257006
[106] Koralek J D *et al* 2006 *Phys. Rev. Lett.* **96** 017005
[107] Borisenko S V *et al* 2003 *Phys. Rev. Lett.* **90** 207001
[108] Cuk T *et al* 2004 *Phys. Rev. Lett.* **93** 117003
[109] Wilson J A 2004 *Phil. Magn.* **84** 2183
[110] Chang J *et al* 2007 *Preprint* cond-mat/0708.2782 v1
[111] Kondo T, Takeuchi T, Tsuda S and Shin S 2006 *Phys. Rev.* B **74** 224511
[112] Yoshida T *et al* 2007 *J. Phys.: Condens. Matter* **19** 125209
[113] Abrahams E and Varma C M 2000 *Proc. Natl Acad. Sci.* **97** 5714
[114] Kikugawa N, Mackenzie A P, Bergemann C and Maeno Y 2004 *Phys. Rev.* B **70** 174501
[115] Lee H-Y 2001 *Phys. Rev.* B **64** 012506
[116] Platé M *et al* 2005 *Phys. Rev. Lett.* **95** 077001
[117] Balakirev F, Betts J B, Migliori A, Ono S, Ando Y and Boebinger G S 2003 *Nature* **424** 912
[118] Tassini L, Venturini F, Zhang Q-M, Hackl R, Kikugawa N and Fujita T 2004 *Preprint* cond-mat/0406169 v2
[119] Bogdanov P V *et al* 2002 *Phys. Rev. Lett.* **89** 167002
[120] Yang K *et al* 2006 *Phys. Rev.* B **73** 144507
[121] Hussey N E, Mackenzie A P, Cooper J R, Maeno Y, Nishizaki S and Fujita T 1998 *Phys. Rev.* B **57** 5505
[122] Baumberger F *et al* 2006 *Phys. Rev. Lett.* **96** 246402
[123] McBrien M N, Hussey N E, Meeson P J, Horii S and Ikuta H 2002 *J. Phys. Soc. Japan* **71** 701
[124] Shulga S V, Dolgov O V and Maksimov E G 1991 *Physica* C **178** 266
[125] Norman M R and Chubukov A V 2006 *Phys. Rev.* B **73** 140501(R)
[126] Hwang J *et al* 2006 *Phys. Rev.* B **73** 014508
[127] Hwang J, Schachinger E, Carbotte J P, Gao F, Tanner D B and Timusk T 2007 *Preprint* cond-mat/0710.4104 v1
[128] Stock C *et al* 2005 *Phys. Rev.* B **71** 024522
[129] Vignolle B *et al* 2007 *Nat. Phys.* **3** 163
[130] Hussey N E, Alexander J C and Cooper R A 2006 *Phys. Rev.* B **74** 214508
[131] Allen P B 1971 *Phys. Rev.* B **3** 305
[132] Waku K, Katsufuji T, Kohsaka Y, Sasagawa T, Takagi H, Kishida H, Okamoto H, Azuma M and Takano M 2004 *Phys. Rev.* B **70** 134501
[133] Gunnarsson O, Calandra M and Han J E 2003 *Rev. Mod. Phys.* **75** 1085
[134] Hussey N E, Takenaka K and Takagi H 2004 *Phil. Mag.* **84** 2847
[135] Kaminski A *et al* 2005 *Phys. Rev.* B **71** 014517
[136] Merino J and McKenzie R H 2000 *Phys. Rev.* B **61** 7996
[137] Takenaka K, Nohara J, Shiozaki R and Sugai S 2003 *Phys. Rev.* B **68** 134501
[138] Wiesmann H, Gurvitch M, Lutz H, Ghosh A K, Schwarz B, Strongin M, Allen P B and Halley J W 1977 *Phys. Rev. Lett.* **38** 782
[139] Yosuf Z, Wells B O, Valla T, Fedorov A V, Johnson P D, Li Q, Kendziora C, Jian S and Hinks D G 2002 *Phys. Rev. Lett.* **88** 167006
[140] Kubo Y, Shimakawa Y, Manako T and Igarashi H 1991 *Phys. Rev.* B **43** 7875
[141] Hussey N E 2005 *J. Phys. Soc. Japan* **74** 1107
[142] Fruchter L, Raffy H, Bouquet F and Li Z Z 2007 *Phys. Rev.* B **75** 092502
[143] Presland M R, Tallon J L, Buckley R G, Liu R S and Flower N E 1991 *Physica* C **176** 95
[144] Kontani H 2006 *J. Phys. Soc. Japan* **75** 013703

[145] Sandemann K G and Schofield A J 2001 *Phys. Rev.* B **63** 094510
[146] Wakimoto S *et al* 2004 *Phys. Rev. Lett.* **92** 217004
[147] Reznik D *et al* 2006 *Nature* **440** 1170
[148] Yelland E A *et al* 2007 *Preprint* cond-mat/0707.0041 v1
[149] Bangura A F *et al* 2007 *Preprint* cond-mat/0707.4461 v1
[150] LeBoeuf D *et al* 2007 *Nature* **450** 533
[151] Rullier-Albenque F, Alloul H, Proust C, Lejay P, Forget A and Colson D 2007 *Phys. Rev. Lett.* **99** 027003
[152] Proust C *et al* unpublished